Three Exceptions to the Grossman-Nir Bound

Robert Ziegler,[1] **Jure Zupan,**[2] **Roman Zwicky**[3]

[1]*Institute for Theoretical Particle Physics (TTP), Karlsruhe Institute of Technology, Engesserstrasse 7, D-76128 Karlsruhe, Germany*

[2]*Department of Physics, University of Cincinnati, Cincinnati, Ohio 45221,USA*

[3]*Higgs Centre for Theoretical Physics, School of Physics and Astronomy, University of Edinburgh, Edinburgh EH9 3JZ, Scotland*

E-mail: robert.ziegler@kit.edu, zupanje@ucmail.uc.edu, roman.zwicky@ed.ac.uk

ABSTRACT: We show that the Grossman-Nir (GN) bound, $\mathrm{Br}(K_L \to \pi^0 \nu\bar\nu) \leq 4.3\,\mathrm{Br}(K^+ \to \pi^+ \nu\bar\nu)$, can be violated in the presence of light new physics with flavor violating couplings. We construct three sample models in which the GN bound can be violated by orders of magnitude, while satisfying all other experimental bounds. In the three models the enhanced branching ratio $\mathrm{Br}(K_L \to \pi^0 + \mathrm{inv})$ is due to $K_L \to \pi^0 \phi_1$, $K_L \to \pi^0 \phi_1 \phi_1$, $K_L \to \pi^0 \psi_1 \bar\psi_1$ transitions, respectively, where $\phi_1(\psi_1)$ is a light scalar (fermion) that escapes the detector. In the three models $\mathrm{Br}(K^+ \to \pi^+ + \mathrm{inv})$ remains very close to the SM value, while $\mathrm{Br}(K_L \to \pi^0 + \mathrm{inv})$ can saturate the present KOTO bound. Besides invisible particles in the final state (which may account for dark matter) the models require additional light mediators around the GeV-scale.

arXiv:2005.00451v2 [hep-ph] 12 May 2020

Contents

1 Introduction

In the SM, the $K_L \to \pi^0 \nu\bar{\nu}$ and $K^+ \to \pi^+ \nu\bar{\nu}$ decays proceed through the same short distance operator, involving the fields of the quark level transition $(s \to d\nu\bar{\nu})$. The matrix elements for the $K_L \to \pi^0 \nu\bar{\nu}$ and $K^+ \to \pi^+ \nu\bar{\nu}$ transitions are thus trivially related through isospin, leading to the Grossman-Nir (GN) bound [1]

$$\mathrm{Br}(K_L \to \pi^0 \nu\bar{\nu}) \leq 4.3 \, \mathrm{Br}(K^+ \to \pi^+ \nu\bar{\nu}). \tag{1.1}$$

The bound remains valid in the presence of heavy New Physics (NP), i.e., for NP modification due to new particles with masses well above the kaon mass. The bound is saturated for the case of maximal CP violation, if lepton flavor violation can be neglected (see Ref. [2] for counter-examples).

In this paper we investigate to what extent NP contributions to $K \to \pi + \text{inv}$ decays can violate the GN bound. Simple dimensional counting shows that for large violations of the GN bound the NP needs to be light, of order of a few GeV at most (see Section 2 and Refs. [3, 4]). Such light NP faces stringent experimental constraints from rare meson decays and collider/beam dump searches as well as from astrophysics and cosmology. Nevertheless, the couplings needed to modify the rare $K \to \pi + \text{inv}$ decays are small enough that interesting modifications of the GN bound are indeed possible. We identify three sample models that achieve this through the following decays:

- Model 1: $K_L \to \pi^0 \phi_1$, where the mass of the light scalar, ϕ_1, can be anywhere from $m_{\phi_1} \lesssim m_K - m_\pi$ to a few MeV or even less,

- Model 2: $K_L \to \pi^0 \phi_1 \phi_1$, where the mass of the light scalar, ϕ_1, is required in a large part of the parameter space to be above $m_{\phi_1} \gtrsim m_\pi/2$ in order to avoid constraints from invisible pion decays,

- Model 3: $K_L \to \pi^0 \psi_1 \bar{\psi}_1$, with ψ_1 a light fermion whose mass is required to be above $m_{\psi_1} \gtrsim m_\pi/2$ in most of the phenomenologically viable parameter space.

The ϕ_1 and ψ_1 particles are feebly interacting and escape the detector, resulting in the $K_L \to \pi^0 + \text{inv}$ signature, as does the SM transition, $K_L \to \pi^0 \nu \bar{\nu}$. The NP is thus detected through an enhanced $\Gamma(K_L \to \pi^0 + \text{inv})$ rate. Furthermore, the three models can be distinguished from the SM and each other by measuring the energy distribution of the neutral pion, $d\Gamma(K_L \to \pi^0 + \text{inv})/dE_\pi$, see Fig. 1 for several sample distributions. While the two body decay in Model 1 results in a fixed pion energy, the three body decays in Model 2 and 3 can be close to the SM distribution for light ϕ_1 and ψ_1 masses and differ from it for non-negligible masses. Let us mention in passing that the lightness of the scalars could be due to them being a pseudo Goldstone boson of a broken global symmetry whereas for fermions light masses are natural due to chiral symmetry.

In all three models the branching ratio $\text{Br}(K^+ \to \pi^+ + \text{inv})$ remains close to the SM value, $\text{Br}(K^+ \to \pi^+ \nu \bar{\nu})_{\text{SM}} = (8.4 \pm 1.0) \times 10^{-11}$ [5–7], and thus below the preliminary NA62 bound $\text{Br}(K^+ \to \pi^+ \nu \bar{\nu})_{\text{exp}} < 1.85 \times 10^{-10}$ [8], while $\text{Br}(K_L \to \pi^0 + \text{inv})$ can be enhanced well above its SM value, $\text{Br}(K_L \to \pi^0 \nu \bar{\nu})_{\text{SM}} = (3.4 \pm 0.6) \times 10^{-11}$ [5–7]. The NP induced $K_L \to \pi^0 + \text{inv}$ transitions can even saturate the present upper experimental bounds from KOTO $\text{Br}(K_L \to \pi^0 \nu \bar{\nu})_{\text{exp}} < 3.0 \times 10^{-9}$ [9].[1]

---

[1]For two body decays the bound is somewhat stronger, $\text{Br}(K_L \to \pi^0 \nu \bar{\nu})_{\text{exp}} < 2.4 \times 10^{-9}$, for $m_{\phi_1} \lesssim m_\pi$ [9]. If the new preliminary data are interpreted as a signal, they instead correspond to a rate of $\text{Br}(K_L \to \pi^0 + \text{inv})_{\text{KOTO}} = \left(2.1^{+2.0}_{-1.1}\right) \times 10^{-9}$ [10, 11] (note though, that some of the observed events are likely due to previously unidentified backgrounds [12]). Furthermore, in the numerics we quote the experimental bounds on three body decays, $K \to \pi \phi_1 \phi_1$ $K \to \pi \psi_1 \bar{\psi}_1$, assuming the experimental efficiencies are the same as for the SM $K \to \pi \nu \bar{\nu}$ transition. In reality, we expect the bounds to be weaker, since the experimental
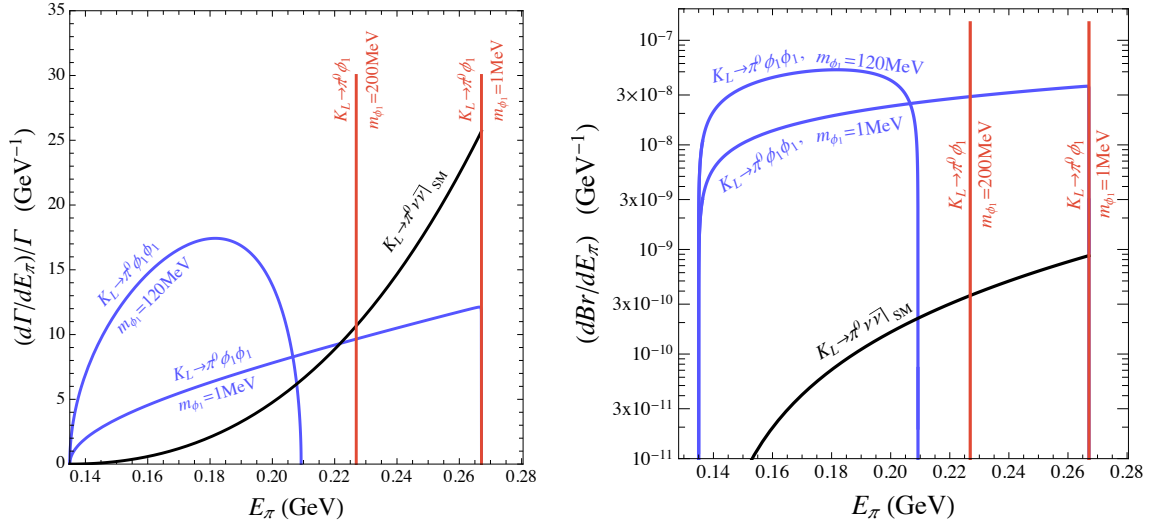
Figure 1. *Left:* The normalized decay width distributions as functions of the pion energy, E_π, for the SM (black line), for the decay dominated by the two body NP transition (Model 1), $K_L \to \pi^0 \phi_1$, for two choices of invisible scalar masses, $m_{\phi_1} = 1$ MeV, 200 MeV (red lines) and for three body NP decay (Model 2), $K_L \to \pi^0 \phi_1 \phi_1$, with $m_{\phi_1} = 1$ MeV, 120 MeV (blue lines). *Right:* The branching ratio distributions, where NP contributions saturate the present KOTO bound [9]. At the kinematic endpoint, $E_\pi \to m_\pi$, we have $d\Gamma_{\rm SM} \propto p_\pi^3 dE_\pi$ while for NP Model 2 $d\Gamma_{K_L \to \pi^0 \phi_1 \phi_1} \propto p_\pi dE_\pi$, where $p_\pi = (E_\pi^2 - m_\pi^2)^{1/2}$ (similarly for Model 3, Section 5, $d\Gamma_{K_L \to \pi^0 \psi_1 \bar\psi_1} \sim p_\pi dE_\pi$ unless the Yukawa couplings y_{ij} are purely real). This follows from the partial wave expansion, $d\Gamma/dE_\pi \sim p_\pi^{2l+1}$, adapted to EFTs [22]. In the $K \to \pi \nu \bar\nu$ rate the V-A SM interaction induces a negligible S-wave contribution proportional to the neutrino mass, whereas the scalar interactions in our model induce a non-suppressed S-wave. The maximum recoil, $E_\pi \to E_\pi\big|_{\rm max}$, in contrast, is controlled by a single power of the ν/ϕ_1-velocity in the q^μ rest frame, $\beta_{\nu,\phi_1} = (1 - 4m_{\nu/\phi_1}^2/q^2)^{1/2}$ (where $q^2 = m_K^2 + m_\pi^2 - 2m_K E_\pi$). For small m_{ν/ϕ_1} this velocity goes to 1 for most values of q^2, leading to a sharp cut-off at $E_\pi\big|_{\rm max}$.

The three models considered in this work differ from the other proposed NP solutions to the KOTO anomaly in that they allow for large violations of the GN bound at the level of the amplitudes already. In contrast, Ref. [13] relies on the fact that the available phase space is larger for neutral kaon decays due to $m_{K_L} - m_{\pi^0} > m_{K^+} - m_{\pi^+}$ and thus $K^+ \to \pi^+ X_{\rm inv}$ decays can be forbidden by a finely tuned choice for the mass of the invisible final state $X_{\rm inv}$. Ref. [11] instead obtains, in one of the models, an apparent violation of the GN bound from the experimental set-up; the produced light NP particles decay on experimental length-scales, and are not observed in NA62 but are observed in KOTO due to the geometry of the experiments. Finally, the NP models of Refs. [11, 14–21] do not violate the GN bound, but can allow for a large signal in KOTO since NA62 is not sensitive to $X_{\rm inv}$ with a mass close to the pion mass.

The paper is organized as follows. In section 2 a general Effective Field Theory analysis

---

efficiencies are highest for larger values of E_π, while NP decays considered here are less peaked towards maximal E_π (as compared to the SM).

is presented. The three models are discussed consecutively in Sections 3, 4 and 5 with the main plots collected in Figs. 5, 6, in Figs. 15, 16 and in Figs. 19, 20 for Model 1, 2 and 3, respectively, with constraints due to $K^0 - \bar{K}^0$ mixing, cosmology and invisible pion decays discussed in the respective sections. The paper ends with conclusions in Section 6, while details on decay rates and integral conventions are deferred to two short appendices.

2 The EFT analysis

We first perform an Effective Field Theory (EFT) based analysis, assuming that the SM is supplemented by a single light scalar, φ, while any other NP states are heavy and integrated out. The light scalar has flavor violating couplings and is created in the $K^0 \to \pi^0 \varphi$ decay. The effective Lagrangian inducing this transition is given by[2]

$$\mathcal{L}_{\text{eff}} = c^{(4)}(\bar{s}d)\varphi + \sum_i \frac{c_i^{(7)}}{\Lambda^3}(\bar{s}\Gamma_i d)(\bar{d}\Gamma'_i d)\varphi + \cdots , \tag{2.1}$$

where we only keep the parity-even operators of lowest dimension and work in the quark mass basis. There is a single dimension 4 operator, and the sum runs over the dimension 7 operators, where Γ_i, Γ'_i include both Dirac and color structures.

At the quark level the dimension 4 operator induces the $s \to d\varphi$ transition and thus contributes equally to $K^0 \to \pi^0 \varphi$ and $K^+ \to \pi^+ \varphi$ decays, see the first diagram in Fig. 2. The resulting matrix elements for the $K_L \to \pi^0 \varphi$ and $K^+ \to \pi^+ \varphi$ decays are

$$\{\mathcal{M}^{(4)}(K_L \to \pi^0 \varphi), \mathcal{M}^{(4)}(K^+ \to \pi^+ \varphi)\} = \frac{m_K^2 - m_\pi^2}{m_s - m_d} f_+(0)\{\text{Im}\, c^{(4)}, c^{(4)}\}. \tag{2.2}$$

The $K_L \to \pi^0 \varphi$ decay is CP violating and vanishes in the limit of zero weak phases, $\text{Im}\, c^{(4)} \to 0$. These contributions therefore obey the Grossman-Nir relation,

$$|\mathcal{M}^{(4)}(K_L \to \pi^0 \varphi)| \leq |\mathcal{M}^{(4)}(K^+ \to \pi^+ \varphi)|. \tag{2.3}$$

The dimension 7 operators, on the other hand, contribute to $K^0 \to \pi^0 \varphi$ and $K^+ \to \pi^+ \varphi$ decays in a qualitatively different way. The $K_L \to \pi^0 \varphi$ decay can proceed through the weak annihilation type contractions of valence quarks, i.e., through the third diagram in Fig. 2. The $K^+ \to \pi^+ \varphi$ transition requires the $\bar{d}d$ internal line to close in a loop (cf. the 2nd diagram in Fig. 2). Such contractions also contribute to $K_L \to \pi^0 \varphi$. Using at first perturbative counting the latter contributions are suppressed, giving parametric estimates

$$\{\mathcal{M}^{(7)}(K_L \to \pi^0 \varphi), \mathcal{M}^{(7)}(K^+ \to \pi^+ \varphi)\} \propto \frac{m_K^3}{\Lambda^3}\left\{\text{Im}\, c_i^{(7)}, \frac{1}{(4\pi)^2}\left(\frac{\alpha_s}{4\pi}\right)^n c_i^{(7)}\right\}, \tag{2.4}$$

where we neglected m_π compared to m_K and do not write factors that are parametrically of the same size but may differ by $\mathcal{O}(1)$, such as different form factors in the two cases.

---

[2]The full Lagrangian is $\mathcal{L} = c_4(\bar{s}d)\varphi + c'_4(\bar{s}\gamma_5 d)\varphi + \cdots$, but we display only the operators that are parity even and thus contribute to the $K \to \pi$ decay. The dimension 5 operator $(\bar{s}\gamma_\mu d)\partial_\mu\varphi$ can be traded for the dimension 4 operator $(m_s - m_d)(\bar{s}d)\varphi$ via equations of motion (EOMs). Similarly, the dimension 6 operator $(\bar{s}\overleftrightarrow{D}_\mu d)\partial^\mu\varphi$ can be traded for $\bar{s}d\varphi$ via EOM, leaving the dimension 4 and dimension 7 operators in (2.1) as operators of lowest dimension.
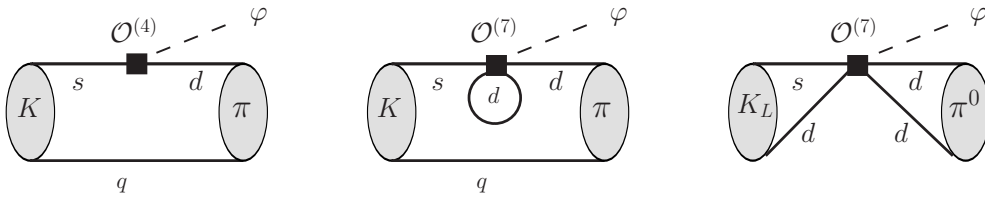
Figure 2. Contributions from dimension 4 (first diagram) and dimension 7 (2nd and 3rd diagrams) EFT operators to the $K \to \pi\varphi$ transition. The last diagram contributes to $K_L \to \pi^0\varphi$ only. The quark-loop diagram in the middle corresponds to the S, E classes of diagrams and the weak annihilation diagram on the right to the W, C classes of diagrams in the lattice computation of Ref. [23].

Depending on the Dirac-color structures $\Gamma_i^{(\prime)}$ of the operator one or more gluon exchanges may be required leading to additional $(\alpha_s/4\pi)^n$-factors shown in (2.4).

A priori this leaves two classes of NP models with potentially sizeable violations of the GN bound. The first possibility is heavy NP, with a suppressed $c^{(4)}$ Wilson coefficient such that dimension 7 operators dominate. The other possibility is light NP such that the EFT assumption, on which the above analysis is based on, is violated.

Building viable heavy NP models that violate the GN bound faces several obstacles. First of all, $c^{(4)}$ would have to be heavily suppressed, $c^{(4)} \ll m_q/\Lambda$, well below naive expectations. If this is not the case, the "heavy" NP scale needs to be quite light. For instance, for $c^{(4)} \sim m_q/\Lambda$, $c_i^{(7)} \sim \mathcal{O}(1)$ the dimension 4 operator contributions dominate over the dimension 7 ones already for $\Lambda \gtrsim \mathcal{O}(3\ \text{GeV})$ (see also the discussion in [3]). Furthermore, even if the hierarchy $c^{(4)} \ll c^{(7)}$ was realised, it is not clear whether the GN bound could be violated by more than a factor of a few. The scaling estimates in (2.4) were based on perturbative expansion, while the kaon decays are in the deep non-perturbative regime of QCD. One can get an idea of the size of the $\mathcal{M}_K^{(7)} \propto \langle \pi\varphi | \mathcal{O}^{(7)} | K \rangle$ matrix elements by linking them to the ones for $K \to \pi\ell^+\ell^-$ decays that were explored in lattice QCD for light quark masses above their physical value ($m_\pi = 430\ \text{MeV}$ and $m_K = 625\ \text{MeV}$) [23]. Figure 5 in Ref. [23] indicates that the quark-loop and weak annihilation contractions, corresponding to the middle and the right diagrams in Fig. 2, lead to contributions of comparable size, contrary to the perturbative expectations in (2.4). If these results carry over to $K \to \pi\varphi$ decays, it would seem that the ratio of $\mathcal{M}^{(7)}(K_L \to \pi^0\varphi)/\mathcal{M}^{(7)}(K^+ \to \pi^+\varphi)$ would not easily exceed a factor of ~ 2 in models of heavy NP. It is unclear, however, whether this qualitative feature, based on the evaluation of the SM $V - A$ four quark operators [23], would carry over to a model with scalar-scalar four quark operators, originating from a scalar mediator. For instance, for $V - A$ operators the weak annihilation topology is chirally suppressed in the factorisation approximation, while this is not the case for scalar operators.

In conclusion, for heavy mediators the GN bound might or might not be violated in the case $c^{(4)} \ll c^{(7)}$. In this manuscript we therefore focus on the second possibility, the possibility of light NP mediators, where we can use Chiral Perturbation Theory (ChPT)
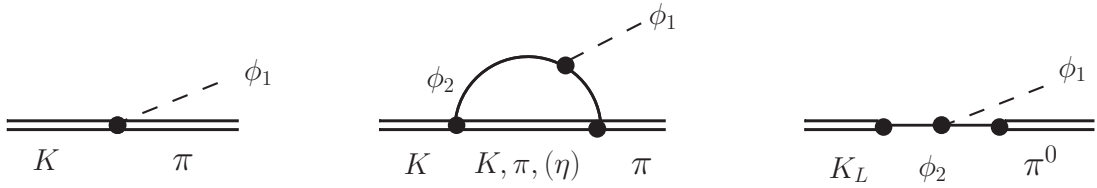
Figure 3. Diagrams for the $K \to \pi \phi_1$ decay in Model 1 with the GN-violating contribution to the very right. These diagrams enter the matrix elements in Eqs. (3.13), (3.14). Note that the η in the loop contributes to the K_L decay only. Diagrams which we neglect, such as the diagrams of $\mathcal{O}(p^4)$ or $\mathcal{O}(g_{qq'}^3)$, are not shown.

with light NP states as a reliable tool to make predictions.

3 Model 1 - scalar model leading to two-body kaon decays

In the first example we introduce two real scalar fields, ϕ_1 and ϕ_2. The enhancement of the $K \to \pi$+inv branching ratio over the SM is due to the $K \to \pi \phi_1$ decay, while $K \to \pi \phi_2$ is kinematically forbidden, i.e., we take $m_{\phi_2} > m_K - m_\pi$. The ϕ_1 interacts feebly with matter and escapes the detector, resulting in a missing momentum signature[3]. The relevant terms in the Lagrangian are

$$\mathcal{L} \supset g_{qq'}^{(i)}(\bar{q}_L q_R')\phi_i + \text{h.c.} + \lambda m_S \phi_2^2 \phi_1 \, , \tag{3.1}$$

where $q, q' = \{u, d, s\}$ and summation over repeated indices is implied. The couplings $g_{qq'}^{(i)}$ are complex, and their imaginary parts trigger the $K_L \to \pi^0 \phi_1$ decay.

Large violations of the GN bound arise when there is a large hierarchy among the following couplings,

$$g_{sd}^{(1)} \ll g_{sd}^{(2)} \ll g_{dd}^{(2)}, \tag{3.2}$$

while all other couplings are further suppressed. In our benchmarks these remaining couplings as well as $g_{sd}^{(1)}$ will be set to zero. Before proceeding to predictions for branching ratios and the numerical analysis, it is instructive to perform a naive dimensional analysis (NDA). This will give us insight into why large violations of the GN bound are possible as well as to how large these violations can possibly be.

Taking $m_S \sim m_{\phi_2} \sim m_K$ the NDA estimate for the two decay amplitudes are,

$$\mathcal{M}(K_L \to \pi^0 \phi_1) \; \propto \; \text{Im } g_{sd}^{(1)} + \mathcal{O}(1) \times \lambda \, \text{Im} \, g_{sd}^{(2)} \, \text{Im} \, g_{dd}^{(2)} \, , \tag{3.3}$$

$$\mathcal{M}(K^+ \to \pi^+ \phi_1) \propto g_{sd}^{(1)} + \mathcal{O}(1) \times \frac{1}{16\pi^2} \lambda \, g_{sd}^{(2)} g_{dd}^{(2)} \, , \tag{3.4}$$

where the first term in each line is due to the 1st diagram in Fig. 3. The second term in (3.3) is due to the 3rd diagram in Fig. 3, which is absent in the $K^+ \to \pi^+ \phi_1$ decay. This

---

[3]The ϕ_1 could also decay to neutrinos, $\phi_1 \to \nu\bar{\nu}$, so that the final state can even be the same as in the SM, though with the $\nu\bar{\nu}$ pair forming a resonant peak. We do not explore this possibility any further.
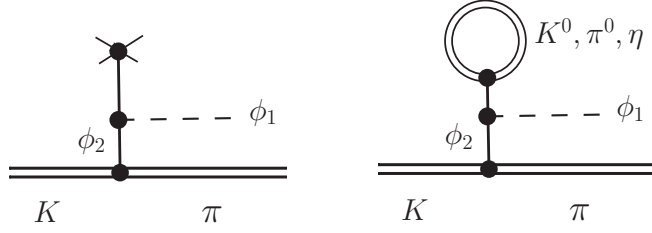
Figure 4. The contributions to the $K \to \pi \phi_1$ decay in Model 1 proportional to $\langle \phi_2 \rangle$ (right), and the related one-loop tadpole diagram (left).

is the crucial difference between the two decays and leads to large violations of the GN bound, provided $g_{sd}^{(1)}$ is small.

However, violations of the GN bound cannot be arbitrarily large. Even if $g_{sd}^{(1)}$ is set to zero, the $K^+ \to \pi^+ \phi_1$ transition is generated at the loop level from the 2nd diagram in Fig. 3, giving the 2nd term in (3.4). Without fine-tuning the ratio $\mathcal{M}(K_L \to \pi^0 \phi_1)/\mathcal{M}(K^+ \to \pi^+ \phi_1)$ is thus at best as large as the loop factor, $16\pi^2 \sim 10^3$. Taking into account the present experimental results, this is more than enough to saturate the present KOTO bound while only marginally modifying the $K^+ \to \pi^+ +$inv decay.

In order to simplify the discussion we assume below that the vacuum expectation values (vevs) of the scalar fields $\phi_{1,2}$ vanish, $\langle \phi_1 \rangle = \langle \phi_2 \rangle = 0$. If this is not the case the $K \to \pi \phi_1$ decays receive additional GN-conserving contributions, see Fig. 4 (right). More precisely, it is the renormalised vevs that are set to zero, $\langle \phi_1 \rangle_{\rm ren} = \langle \phi_2 \rangle_{\rm ren} = 0$, since we work to one loop order. That is, we set the sum of the two diagrams in Fig. 4 to be zero. Had we set them instead to their natural value, $\langle \phi_i \rangle_{\rm ren} \sim m_K g_{dd}^{(i)}/16\pi^2$, our results would not change qualitatively. While $\mathcal{M}(K^+ \to \pi^+ \phi_1)$ would be modified by an $\mathcal{O}(1)$ factor, in $\mathcal{M}(K_L \to \pi^0 \phi_1)$ such contributions are always subleading and one would thus still have large violations of the GN bound.

3.1 Estimating the transition rates using ChPT

We use ChPT to calculate the transition rates. In constructing the ChPT we count $\phi_1 \sim \phi_2 \sim \mathcal{O}(p)$.[4] As far as QCD is concerned $\phi_{1,2}$ are external sources and can be treated as spurions [24, 25] when building the low energy effective Lagrangian. The QCD Lagrangian, including (3.1), can be conveniently rewritten as,

$$\mathcal{L}_{\rm QCD+\phi} = \bar{q}(i\slashed{\partial} + g_s \slashed{G}^a T^a)q - \bar{q}\mathcal{M}_q q - \sum_i \phi_i \, \bar{q}(\chi_S^{(i)} - i\chi_P^{(i)}\gamma_5)q, \qquad (3.5)$$

___

[4]That is, we count m_{ϕ_1} and m_{ϕ_2} both as $\mathcal{O}(p) \sim m_K - m_\pi$, even though ϕ_2 is $m_K - m_\pi$ by a factor of a few in large part of the parameter space that we consider. Hence for heavy ϕ_2 our ChPT based results should be taken as indicative only and could receive corrections of $\mathcal{O}(1)$. Since we only wish to demonstrate that large deviations of the GN bound are possible this suffices. However, should an anomalously large $K_L \to \pi^0 +$inv rate be experimentally established our results should be revisited, say, for m_{ϕ_2} towards and above 1 GeV.

where we keep only the light quarks, $q = (u, d, s)$. The diagonal mass matrix is $\mathcal{M}_q = \text{diag}(m_u, m_d, m_s)$, while $\chi_{S,P}^{(i)}$ are 3×3 Hermitian matrices describing the quark couplings to $\phi_{1,2}$,

$$\left[\chi_S^{(i)}\right]_{qq'} = -\frac{1}{2}\big(g_{qq'}^{(i)} + g_{q'q}^{(i)*}\big), \qquad \left[\chi_P^{(i)}\right]_{qq'} = -\frac{i}{2}\big(g_{qq'}^{(i)} - g_{q'q}^{(i)*}\big) . \tag{3.6}$$

Since we set the couplings to the up quark to zero they have the following form[5]

$$\chi_S^{(i)} = -\begin{pmatrix} 0 & 0 & 0 \\ 0 & \text{Re}\, g_{dd}^{(i)} & \bar{g}_{ds}^{(i)} \\ 0 & \bar{g}_{sd}^{(i)} & \text{Re}\, g_{ss}^{(i)} \end{pmatrix}, \qquad \chi_P^{(i)} = \begin{pmatrix} 0 & 0 & 0 \\ 0 & \text{Im}\, g_{dd}^{(i)} & \hat{g}_{ds}^{(i)} \\ 0 & \hat{g}_{sd}^{(i)} & \text{Im}\, g_{ss}^{(i)} \end{pmatrix}. \tag{3.7}$$

The off-diagonal couplings in (3.7),

$$\bar{g}_{ds}^{(i)} = \bar{g}_{sd}^{(i)*} = \tfrac{1}{2}\big(g_{ds}^{(i)} + g_{sd}^{(i)*}\big), \qquad \hat{g}_{ds}^{(i)} = \hat{g}_{sd}^{(i)*} = -\tfrac{i}{2}\big(g_{ds}^{(i)} - g_{sd}^{(i)*}\big), \tag{3.8}$$

are the origin of the flavor violations.

The Lagrangian for QCD with the flavor violating $\phi_{1,2}$, $\mathcal{L}_{\text{QCD}+\phi}$, is formally invariant under a global $SU(3)_R \times SU(3)_L$ transformation, $q_{R,L} \to g_{R,L} q_{R,L}$, provided $\chi_{S,P}^{(i)}\phi_i$ and $\mathcal{M}_q$ are promoted to spurions transforming as

$$s + ip \to g_R(s + ip)g_L^\dagger, \tag{3.9}$$

where s and p stand for

$$s = \mathcal{M}_q + \sum_i \chi_S^{(i)}\phi_i, \qquad p = \sum_i \chi_P^{(i)}\phi_i, \tag{3.10}$$

with $\chi_{S,P}^{(i)}$ given in (3.7).

The LO ChPT Lagrangian, with $\phi_{1,2}$ included as light degrees of freedom, is given by

$$\begin{aligned}
\mathcal{L}_{\text{ChPT}+\phi}^{(2)} &= \frac{f^2}{4}\text{Tr}\big(\partial_\mu U \partial^\mu U^\dagger\big) + B_0\frac{f^2}{2}\,\text{Tr}\left[(s - ip)U + (s + ip)U^\dagger\right] \\
&\quad + \frac{1}{2}\partial_\mu\phi_i\partial^\mu\phi_i - \frac{m_{\phi_i}^2}{2}\phi_i^2 + \lambda m_S\phi_2^2\phi_1 + \cdots ,
\end{aligned} \tag{3.11}$$

where the ellipses stand for additional terms in the scalar potential. Here $U(x) = \exp(i\lambda^a\pi^a/f)$ is the unitary matrix parametrizing the meson fields [24, 25], B_0 is a constant related to the quark condensate, $B_0(\mu = 2\,\text{GeV}) = 2.666(57)\,\text{GeV}$, f is related to the pion decay constant $f \simeq f_\pi/\sqrt{2} = 92.2(1)\,\text{MeV}$ [26], with normalization $\langle 0|\bar{u}\gamma_\mu\gamma_5 d(0)|\pi^-(p)\rangle = ip_\mu f_\pi$. The kaon decay constant $f_K = 155.6 \pm 0.4\,\text{MeV}$ [27] accommodates SU(3) breaking at times.

In this paper we work to partial NLO order: all LO terms in the chiral expansion $\mathcal{O}(p^2)$ are kept, as well as the one loop corrections which are of order $\mathcal{O}(p^4)$ and all finite.

---

[5]For light ϕ_2, which is our preferred scenario, assuming $g_{uu}^{(2)} \neq 0$ would not introduce new qualitative features. According to chiral counting, $g_{uu}^{(2)} \neq 0$ induces a $K^+\pi^-\phi_1$-term at $\mathcal{O}(p^4)$, and is thus subleading to $K_L\pi^0\phi_1$-terms that we consider. Hence we set $g_{uu}^{(2)}$ to zero for simplicity rather than necessity.

The complete $\mathcal{O}(p^4)$-expressions for decay amplitudes involves additional contact terms (counter-terms or low energy constants), parametrically of the same size as the one loop corrections. However, since $\phi_{1,2}$ are propagating degrees of freedom in our EFT the values of the low energy constants in $\mathcal{O}(p^4)$-ChPT are generally different from the ones in pure QCD and therefore unknown. The associated error in $K_L \to \pi^0\phi_1$ is small, since the NLO corrections are always subleading, while in $K^+ \to \pi^+\phi_1$ they could give $\mathcal{O}(1)$ corrections but would not invalidate our conclusions. For simplicity they are set to zero throughout and we do not discuss them any further.

Next we calculate the $K \to \pi\phi_1$ decay amplitudes. Expanding in the meson fields the $\mathcal{O}(p^2)$ Lagrangian reads

$$
\begin{aligned}
\mathcal{L}^{(2)}_{\text{ChPT}+\phi} \supset\ & B_0 f \sum_i \phi_i \Big(\sqrt{2}\hat{g}^{(i)}_{ds}\bar{K}^0 + \sqrt{2}\hat{g}^{(i)}_{sd}K^0 - \operatorname{Im} g^{(i)}_{dd}\pi^0 + \tfrac{1}{\sqrt{3}}\operatorname{Im}\big(g^{(i)}_{dd} - 2g^{(2)}_{ss}\big)\eta \Big) \\
& + B_0 \sum_i \phi_i \Big\{ \operatorname{Re}(g^{(i)}_{dd}+g^{(i)}_{ss})K^0\bar{K}^0 + \operatorname{Re}(g^{(i)}_{dd})\big(\tfrac{1}{2}(\pi^0)^2 - \tfrac{1}{\sqrt{3}}\eta\pi^0\big)+ \\
& + \operatorname{Re} g^{(i)}_{ss}K^+K^- + \operatorname{Re} g^{(i)}_{dd}\pi^+\pi^- + \\
& + \Big[\bar{g}^{(i)}_{sd}\big(-\tfrac{1}{\sqrt{2}}K^0\pi^0 + K^+\pi^- - \tfrac{1}{\sqrt{6}}K^0\eta\big) + \text{h.c.}\Big] + \cdots \Big\} ,
\end{aligned}
\tag{3.12}
$$

where we only kept terms relevant for the calculation of the $K \to \pi\phi_1$ transition, and the analysis of experimental bounds on the ϕ_1-couplings.

The NP contributions to the decay amplitude for the $K_L \to \pi^0\phi_1$ and $K^+ \to \pi^+\phi_1$ transitions are, see Fig. 3,

$$
\begin{aligned}
\mathcal{M}(K_L \to \pi^0\phi_1)_{\text{NP}} = \Big\{ & 2\operatorname{Im}\hat{g}^{(2)}_{sd}\operatorname{Im} g^{(2)}_{dd}\Delta_{\phi_2}(m_K^2)\Delta_{\phi_2}(m_\pi^2)\lambda m_S B_0 f_K f_\pi \\
& + \operatorname{Im}\bar{g}^{(1)}_{sd} - \frac{\operatorname{Im}\bar{g}^{(2)}_{sd}}{8\pi^2}\lambda m_S B_0 \mathcal{F}^{(2)}_L(I) \Big\} B_0 ,
\end{aligned}
\tag{3.13}
$$

$$
\mathcal{M}(K^+ \to \pi^+\phi_1)_{\text{NP}} = -\Big\{ \bar{g}^{(1)}_{sd} - \frac{\bar{g}^{(2)}_{sd}}{8\pi^2}\lambda m_S B_0 \mathcal{F}^{(2)}_+(I) \Big\} B_0 ,
\tag{3.14}
$$

where $\Delta_X(k^2) \equiv 1/(k^2 - m_X^2)$ hereafter and

$$
\mathcal{F}^{(2)}_L(Y) = \operatorname{Re} g^{(2)}_{ss}Y(m_K) + \operatorname{Re} g^{(2)}_{dd}\big(Y(m_K) + Y(m_\pi) - \tfrac{1}{3}Y(m_\eta)\big) ,
\tag{3.15}
$$

$$
\mathcal{F}^{(2)}_+(Y) = \operatorname{Re} g^{(2)}_{ss}Y(m_K) + \operatorname{Re} g^{(2)}_{dd}Y(m_\pi) ,
\tag{3.16}
$$

are structures occurring in all three models. They depend on the loop function $I(m_X) = C_0(m_K^2, m_{\phi_1}^2, m_\pi^2, m_X^2, m_{\phi_2}^2, m_{\phi_2}^2)$, with C_0 the standard scalar three-point Passarino-Veltman function (cf. App. B). In the $m_{\phi_2} \gg m_K, m_X$ limit we have $I(m_X) \to -1/m_{\phi_2}^2$. Moreover, the replacement $f^2 \to f_\pi f_K/2$ accounts for the main SU(3) breaking effects.

Note that the amplitude vanishes in the limit of no CP violation, $\operatorname{Im}\hat{g}^{(i)}_{sd}, \operatorname{Im}\bar{g}^{(i)}_{sd} \to 0$. The first term in (3.13), proportional to $\hat{g}^{(2)}_{sd}$, is the $\mathcal{O}(p^2)$ contribution due to the tree level exchange of ϕ_2, see the 3rd diagram in Fig. 3. It is isospin violating since it gives rise to the $K_L \to \pi^0\phi_1$ transition but not to $K^+ \to \pi^+\phi_1$. The first term in the second line of Eq. (3.13) is the remaining $\mathcal{O}(p^2)$ contribution, due to the emission of ϕ_1 directly from the

meson line, see the 1st diagram in Fig. 3. This contribution is isospin conserving – it is present for both $K_L \to \pi^0\phi_1$ and $K^+ \to \pi^+\phi_1$ transitions. It is proportional to $\bar{g}_{sd}^{(1)}$ and is thus small due to the assumed hierarchy among the couplings, Eq. (3.2).

The hierarchy of couplings $|g_{sd,ds}^{(2)}| \gg |g_{sd,ds}^{(1)}|$ thus leads to maximal violation of the GN bound by NP contributions. However, this violation cannot be arbitrarily large. Even in the $\bar{g}_{sd}^{(1)} \to 0$ limit we still have isospin conserving NP contributions generated at one loop, see the 2nd diagram in Fig. 3, giving the last term in (3.13). If ϕ_2 is heavy and integrated out these radiative corrections match onto the $\phi_1 - K\pi$ vertex, which is then radiatively induced. Moreover the $K_L \to \pi^0\phi_1$ and $K^+ \to \pi^+\phi_1$ decays receive contributions from $\pi^0 - \phi_1$ mixing where flavor violation comes from the SM $K \to \pi\pi$ transition. For our choices of parameters these contributions are always negligible.

The NP contributions add coherently to the SM rate,

$$\Gamma(K_L \to \pi^0 + \text{inv}) = \Gamma(K_L \to \pi^0\nu\bar{\nu})_{\text{SM}} + \Gamma(K_L \to \pi^0\phi_1)_{\text{NP}}, \qquad (3.17)$$

and the partial decay width due to NP is

$$\Gamma(K_L \to \pi^0\phi_1)_{\text{NP}} = \frac{1}{8\pi}\big|\mathcal{M}(K_L \to \pi^0\phi_1)_{\text{NP}}\big|^2 \frac{p_\pi}{m_K^2}, \qquad (3.18)$$

where $p_\pi = \lambda^{1/2}(m_K^2, m_\pi^2, m_{\phi_1}^2)/(2m_K)$ is the pion's momentum in the K_L rest frame and $\lambda(x,y,z) = x^2 + y^2 + z^2 - 2xy - 2xz - 2yz$ the kinematic Källén function. The expressions for the $K^+ \to \pi^+ + \text{inv}$ decay is completely analogous. Numerically, this gives (the SM predictions are taken from Refs. [5–7, 28])

$$\begin{aligned}
\text{Br}(K_L \to \pi^0 + \text{inv}) = &\underbrace{(3.4 \pm 0.6) \times 10^{-11}}_{\text{SM}} \\
&+ \underbrace{6.0 \times 10^{-9} \left(\frac{\text{Im}\,\hat{g}_{sd}^{(2)}}{5 \cdot 10^{-9}}\right)^2 \left(\frac{\text{Im}\,g_{dd}^{(2)}}{10^{-3}}\right)^2 \left(\frac{\lambda m_S}{1\,\text{GeV}}\right)^2 \left(\frac{1\,\text{GeV}}{m_{\phi_2}}\right)^8}_{\text{NP}},
\end{aligned} \qquad (3.19)$$

where we kept only the leading term for the NP contribution. The typical values of the inputs parameters for the NP contribution were chosen such that they reproduce roughly the KOTO anomaly (in fact slightly larger, but within 1σ). Note the very high scaling in the ϕ_2 mass, underscoring that ϕ_2 needs to be relatively light in order to have large violations of the GN bound. For the charged kaon decay the numerical result is

$$\text{Br}(K^+ \to \pi^+ + \text{inv}) = \underbrace{(8.4 \pm 1.0) \times 10^{-11}}_{\text{SM}} + \underbrace{5.0 \times 10^{-11}\left|\frac{\bar{g}_{sd}^{(1)}}{10^{-13}}\right|^2}_{\text{NP}}, \qquad (3.20)$$

where in the NP contribution we only kept the tree level term and set the value of $\bar{g}_{sd}^{(1)}$ to be similar to the one-loop threshold correction $\bar{g}_{sd}^{(1)} \sim \bar{g}_{sd}^{(2)}g_{dd}^{(2)}/8\pi^2$, cf. Eq. (3.14), with the typical values of the later couplings as in (3.19). While the correction to $K^+ \to \pi^+ + \text{inv}$ is $\mathcal{O}(1)$ of the SM branching ratio, the correction to $K_L \to \pi^0 + \text{inv}$ can be orders of

magnitude above the SM, giving large violations of the GN bound. Note that NP in Model 1 contributes to the 2-body decay $K^+ \to \pi^+ + X^0$ only, and for massless X^0 is subject to the bound $\mathrm{Br}(K^+ \to \pi^+ + X^0) < 0.73 \times 10^{-10}$ from E949 [29], which is slightly stronger than the preliminary NA62 bounds on the 3-body decay $\mathrm{Br}(K^+ \to \pi^+ + \mathrm{inv})_{\mathrm{exp}} < 2.44 \times 10^{-10}$ and the 2-body decay $\mathrm{Br}(K^+ \to \pi^+ + X^0)_{\mathrm{exp}} \lesssim 1.9 \times 10^{-10}$ (for massless X^0) [8].

3.2 Constraints on $\hat{g}_{ds}^{(i)}$ from $K^0 - \bar{K}^0$ mixing

The $K^0 - \bar{K}^0$ mixing is an important constraint on the model. The contributions to the meson mixing matrix element are

$$
M_{12} = M_{12}^{\mathrm{SM}} + M_{12}^{\mathrm{NP}} = -\frac{1}{2m_K}\langle K^0|\mathcal{L}_{\mathrm{eff}}^{\mathrm{SM}}(0)|\bar{K}^0\rangle - \frac{i}{4m_K} \times
$$
$$
\times \int d^4x \langle K^0|T\mathcal{L}_{\mathrm{ChPT}+\phi}^{(2)}(x), \mathcal{L}_{\mathrm{ChPT}+\phi}^{(2)}(0)\}|\bar{K}^0\rangle + \cdots,
\tag{3.21}
$$

where the tree-level exchanges of ϕ_2 is

$$
M_{12}^{\mathrm{NP}} = -\frac{(\hat{g}_{ds}^{(2)} B_0 f_K)^2}{2m_K(m_{\phi_2}^2 - m_K^2)} + \cdots,
\tag{3.22}
$$

with the ellipses denoting higher order terms (we also neglect the NP contributions to the absorptive mixing amplitude since it only enters at one loop). The replacement $f \to f_K/\sqrt{2}$ accounts for the SU(3) breaking.

We consider two constraints, Δm_K and ϵ_K which are CP conserving and CP violating respectively. Using the relation $\Delta m_K = 2\mathrm{Re}M_{12}$ and conservatively assuming, due to the relatively uncertain SM predictions of Δm_K, that the NP saturates the measured Δm_K, we obtain in the limit $m_{\phi_2} \gg m_K$,

$$
\frac{\Delta m_K}{m_K} \simeq 0.69 \big| \mathrm{Re}(\hat{g}_{ds}^{(2)}) \big| \left(\frac{1 \text{ GeV}}{m_{\phi_2}}\right)^2,
\tag{3.23}
$$

and with the experimental value $\Delta m_K^{\mathrm{expt.}} = 3.484(6) \times 10^{-12}$ MeV [27], this translates to

$$
\sqrt{\big| \mathrm{Re}(\hat{g}_{ds}^{(2)}) \big|} < 1.0 \cdot 10^{-7} \times \left(\frac{m_{\phi_2}}{1 \text{ GeV}}\right).
\tag{3.24}
$$

To obtain the bounds on non-SM CP violating contributions to $K^0 - \bar{K}^0$ mixing we use the normalized quantity

$$
C_{\varepsilon_K} = \frac{|\epsilon_K^{\mathrm{SM}+a}|}{|\epsilon_K^{\mathrm{SM}}|}.
\tag{3.25}
$$

For the theoretical prediction of ϵ_K we use the expression [30]

$$
\epsilon_K = e^{i\phi_\epsilon} \sin\phi_\epsilon \left(\frac{\mathrm{Im}\,M_{12}}{\Delta m_K} + \xi\right),
\tag{3.26}
$$

where

$$
\xi \simeq \frac{\mathrm{Im}\,\Gamma_{12}}{\Delta \Gamma_K}.
\tag{3.27}
$$

We take the values for $\Delta m_K = m_L - m_S$, $\Delta \Gamma_K = \Gamma_S - \Gamma_L$, and $\phi_\epsilon = \arctan(2\Delta m_K / \Delta \Gamma_K)$ from experiment [27]. With the SM prediction for $|\epsilon_K|$ from [31], and the NP contribution to M_{12}, Γ_{12} from Eq. (3.22) we get

$$\delta C_{\epsilon_K} = C_{\epsilon_K} - 1 = -5.8 \times 10^{16} \, \text{Im} \left[(\hat{g}_{ds}^{(2)})^2 \right] \left(\frac{1 \, \text{GeV}}{m_{\phi_2}} \right)^2 , \qquad (3.28)$$

The global CKM fit by the UTFit collaboration results in $0.87 < C_{\epsilon_K} < 1.39$ at 95% CL [32, 33], which translates to the following 1σ bounds

$$-(2.6 \times 10^{-9})^2 \left(\frac{m_{\phi_2}}{1 \, \text{GeV}} \right)^2 < \text{Im} \left[(\hat{g}_{ds}^{(2)})^2 \right] < (1.5 \times 10^{-9})^2 \left(\frac{m_{\phi_2}}{1 \, \text{GeV}} \right)^2 . \qquad (3.29)$$

These bounds will improve in the future, once the improved prediction for ϵ_K [31] is implemented in the global CKM fits.

3.3 Constraints on representative benchmarks

To highlight the typical values of couplings that can lead to sizable correction in $K \to \pi +$ inv decays, while passing all other constraints, we form a benchmark 1 (BM1) and a benchmark 2 (BM2),

$$\textbf{BM 1}: \qquad g_{dd}^{(2)} = \frac{(1+i)}{\sqrt{2}} g_{dd} \, , \quad \bar{g}_{sd}^{(2)} = \hat{g}_{sd}^{(2)} = \frac{(1+i)}{\sqrt{2}} g_{sd} \, , \qquad (3.30)$$

$$\textbf{BM 2}: \qquad g_{dd}^{(2)} = i g_{dd} \, , \qquad \bar{g}_{sd}^{(2)} = 0 \, , \quad \hat{g}_{sd}^{(2)} = i g_{sd} \, . \qquad (3.31)$$

These depend on two real parameters, g_{dd} and g_{sd}, parametrizing couplings of ϕ_2 to quarks. All the remaining couplings of ϕ_2 to quarks as well as all the direct couplings of ϕ_1 to quarks are set to zero in accordance with previous discussions. The triple scalar coupling is fixed to $\lambda_S m_S = 1$ GeV (and other potentially relevant scalar couplings assumed to be small, see Section 3.4.1). The mass of ϕ_1 is taken to be small, $m_{\phi_1} = 1$ MeV, while m_{ϕ_2} is kept as a free parameter that is varied in the range $m_{\phi_2} \in [0.4, 1.5]$ GeV, cf. footnote 4.

The form of couplings in BM1, Eq. (3.30), is such that the NP contributions to ϵ_K are maximized. This benchmark is thus representative of the parameter space that is most constrained. Fixing $g_{dd} = 10^{-3}$ the allowed regions are shown in Fig. 5. The red regions are excluded by the NA62 bound on $\text{Br}(K^+ \to \pi^+ \phi_1)_{\text{exp}} \lesssim 1.9 \times 10^{-10}$ [8], the E949 bound $\text{Br}(K^+ \to \pi^+ \phi_1)_{\text{exp}} < 0.73 \times 10^{-10}$ [29] and by the KOTO bound $\text{Br}(K_L \to \pi^0 \phi_1) < 2.4 \times 10^{-9}$ [9]. The E949 and NA62 bounds shown are for massless ϕ_1, which is a good approximation for our benchmarks, where $m_{\phi_1} = 1$ MeV. For heavier masses, above m_π, the bound is expected to become significantly weaker and completely disappear for $m_{\phi_1} \simeq m_{\pi^0}$, as in [34]. The green bands denote the 1σ bands of the branching ratio $\text{Br}(K_L \to \pi^0 + \text{inv})_{\text{KOTO}} = \left(2.1^{+2.0}_{-1.1} \right) \times 10^{-9}$ [10, 11] that corresponds to the anomalous KOTO events. The blue line denotes the GN bound, showing that large violations of the GN bound are possible in this model.

This violation is most apparent in Fig. 5 (right) which gives the allowed values of g_{sd} as a function of m_{ϕ_2}, with the dashed lines denoting contours of the ratio $\text{Br}(K_L \to \pi^0 + \text{inv})/\text{Br}(K^+ \to \pi^+ + \text{inv})$. The present KOTO bound is saturated by values for this
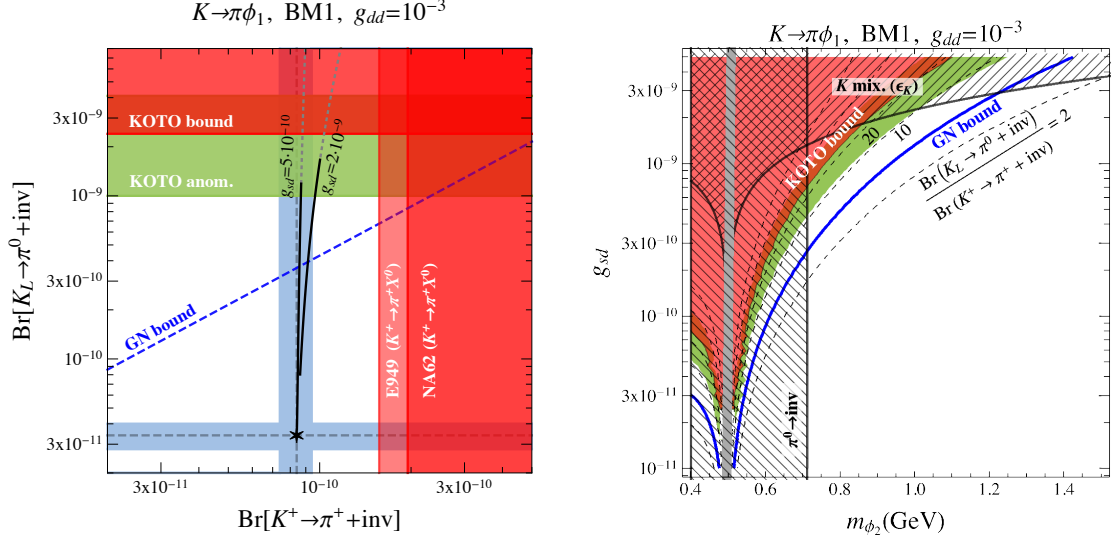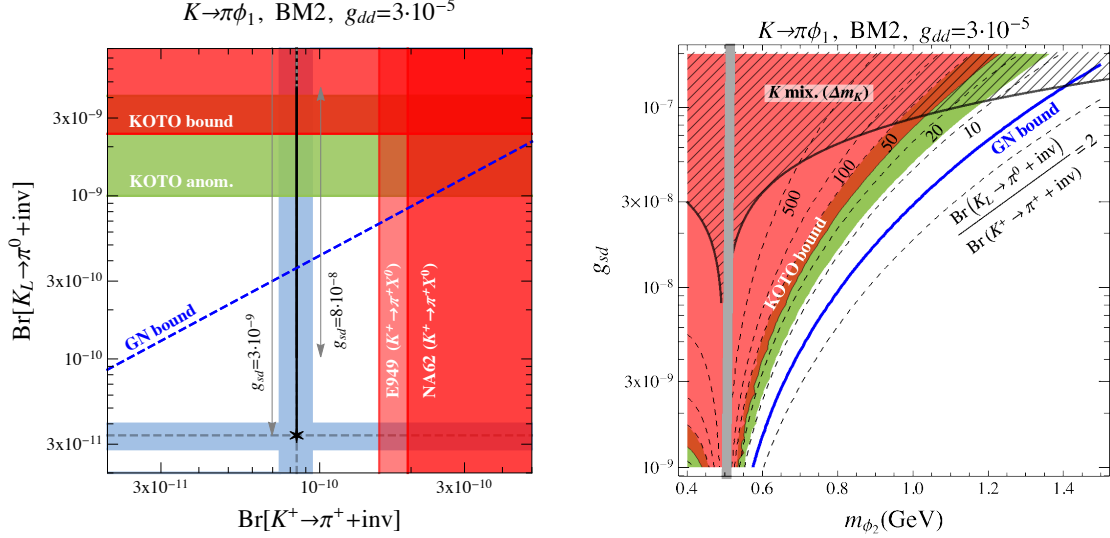
Figure 5. The parameter space for Model 1, BM1, for $g_{dd} = 10^{-3}$ in (3.30). The GN bound is denoted with blue lines, while the green regions give the 1σ bands corresponding to KOTO anomalous events [10, 11]. Left: the predictions for $\mathrm{Br}(K^+ \to \pi^+ + \mathrm{inv})$, $\mathrm{Br}(K_L \to \pi^0 + \mathrm{inv})$, varying $m_{\phi_2} \in [0.4, 1.5]$ GeV and for two values of g_{sd} (black lines). The values closest to the SM (black cross) are reached for $m_{\phi_2} = 1.5$ GeV. Blue regions are the 1σ SM prediction bands, with the central values denoted by the dashed lines and a star, red regions are excluded by NA62 [35], E949 [29] and KOTO [9]. Right: Contours of $\mathrm{Br}(K_L \to \pi^0 + \mathrm{inv})/\mathrm{Br}(K^+ \to \pi^+ + \mathrm{inv})$ (dashed lines) as functions of g_{sd}, m_{ϕ_2}, with the hatched regions excluded by $K^0 - \bar{K}^0$ mixing and $\pi^0 \to inv$ bounds. The region around the kaon mass is masked out (gray region).

ratio of around 20, while still satisfying the ϵ_K constraint, Eq. (3.29), and the $\pi^0 \to$ inv constrain discussed below, see Eq. (3.34). The excluded regions are shown hatched in Fig. 5 (right).

The solid black lines in Fig. 5 (left) show the values of $\mathrm{Br}(K_L \to \pi^0 + \mathrm{inv})$ and $\mathrm{Br}(K^+ \to \pi^+ + \mathrm{inv})$ for $g_{sd} = 5 \cdot 10^{-10}$ and $g_{sd} = 2 \cdot 10^{-9}$, varying $m_{\phi_2} \in [0.4, 1.5]$ GeV, while fixing $g_{dd} = 10^{-3}$ (the grey dotted parts of the lines are excluded by a combination of $K^0 - \bar{K}^0$ and $\pi^0 \to$ inv constraints). The SM predictions for the two branching ratios, $\mathrm{Br}(K^+ \to \pi^+ \nu\bar{\nu})_{\mathrm{SM}} = (8.4 \pm 1.0) \times 10^{-11}$ and $\mathrm{Br}(K_L \to \pi^0 \nu\bar{\nu})_{\mathrm{SM}} = (3.4 \pm 0.6) \times 10^{-11}$ [5–7], are denoted with blue bands (1σ ranges). For the larger value, $g_{sd} = 2 \cdot 10^{-9}$, the prediction is still quite far away from the SM for $m_{\phi_2} = 1.5$ GeV, but would of course tend to the SM for $m_{\phi_2} \to \infty$. For larger values of g_{sd} deviations from the SM prediction for $\mathrm{Br}(K^+ \to \pi^+ + \mathrm{inv})$ at the level of a few are predicted for this benchmark and subject to the indicated constraints from E949, while for smaller values of g_{sd} the deviations in $\mathrm{Br}(K^+ \to \pi^+ + \mathrm{inv})$ become negligibly small. That is, it is possible to explain the KOTO anomalous events without having any appreciable NP effects in the charged kaon decay nor in $K^0 - \bar{K}^0$ mixing.

We next move to BM2. The form of couplings in Eq. (3.31) was deliberately chosen such that there is no NP CP violation in $K^0 - \bar{K}^0$ mixing, in order to avoid the ϵ_K bound.

Figure 6. The preferred parameter space for Model 1, BM2. Color coding is the same as in Fig. 5. See end of Section 3.3 for comments on these figures.

The bound from Δm_K, Eq. (3.24), on CP conserving contributions to $K^0 - \bar{K}^0$ mixing is much weaker, giving the hatched excluded region in Fig. 6 (right). This means that for the same mass of ϕ_2 the flavor violating couplings to quarks can be much larger than in BM1. In Fig. (right) 6 we show the $g_{dd} = 3 \times 10^{-5}$ slice of the parameter space, in which case g_{sd} can be as large as 10^{-7}. Furthermore, the form of couplings in BM2, Eq. (3.31), is such that there is no NP effect at all in $\mathrm{Br}(K^+ \to \pi^+ + \mathrm{inv})$, to the order we are working, and the E949 bound is completely avoided. In contrast, the effect on $\mathrm{Br}(K_L \to \pi^0 + \mathrm{inv})$ can be very large and easily saturate KOTO's present upper bound, as shown for two representative couplings $g_{sd} = 3 \times 10^{-9}, 8 \times 10^{-8}$ (black lines, with dashed parts of the lines excluded by Δm_K). BM2 comes with enhanced symmetry; ϕ_2 is a pure pseudoscalar and ϕ_1 a pure scalar. This has implications for flavor conserving couplings of ϕ_1, to which we turn next.

3.4 Constraints on the ϕ_1-couplings

So far the scalar mass ϕ_1 has been fixed to 1 MeV. Next, we show that for the two benchmarks the radiatively generated couplings of ϕ_1 to pions, nucleons, and photons are all well below the bounds for a large range of ϕ_1 masses (including $m_{\phi_1} = 1$ MeV). Figs. 5 and 6 are thus valid for a larger set of ϕ_1 masses, as long as $m_{\phi_1} \ll m_K$.

3.4.1 Invisible pion decays

If kinematically allowed, $\pi^0 \to \phi_1 \phi_1$ can be an important phenomenological constraint. In Model 1 this decay can proceed through $\phi_2 - \pi^0$ mixing though the loop diagram shown in Fig. 12 (left). In the $m_{\phi_2} \gg m_{\pi,\eta}$ limit the decay amplitude is

$$\mathcal{M}(\pi^0 \to \phi_1 \phi_1) = \frac{1}{12\pi^2} \frac{(\lambda m_S)^2 B_0^2 f}{m_{\phi_2}^4} \operatorname{Re} g_{dd}^{(2)} \left(2 \operatorname{Im} g_{dd}^{(2)} - \operatorname{Im} g_{ss}^{(2)} \right). \qquad (3.32)$$

The corresponding width is given by

$$\Gamma(\pi^0 \to \phi_1\phi_1) = \frac{|\mathcal{M}|^2}{32\pi m_\pi}\beta_{\phi_1}, \tag{3.33}$$

where here $\beta_{\phi_1} \equiv \left(1 - 4m_{\phi_1}^2/m_\pi^2\right)^{1/2}$, so that in the limit $m_{\phi_1} \ll m_\pi \ll m_{\phi_2}$, one has for the branching ratio (setting $\mathrm{Im}\, g_{ss}^{(2)} = 0$ for simplicity)

$$\mathrm{Br}(\pi^0 \to \phi_1\phi_1) = 1.2 \times 10^{-9} \left(\frac{\mathrm{Re}\, g_{dd}^{(2)}}{10^{-3}}\right)^2 \left(\frac{\mathrm{Im}\, g_{dd}^{(2)}}{10^{-3}}\right)^2 \left(\frac{\lambda m_S}{\mathrm{GeV}}\right)^4 \left(\frac{\mathrm{GeV}}{m_{\phi_2}}\right)^8. \tag{3.34}$$

The preliminary 90% C. L. experimental bound reported very recently by NA62 [8]

$$\mathrm{Br}(\pi^0 \to \phi_1\phi_1) < 4.4 \times 10^{-9}, \tag{3.35}$$

improves the E949 bound of 2.7×10^{-7} [36] by almost two orders of magnitude. BM2 obeys this bound trivially, since $\pi^0 \to \phi_1\phi_1$ if forbidden by parity $(\mathrm{Re}\, g_{dd}^{(2)}) = 0)$. For BM1, on the other hand, the bound on $\mathrm{Br}(\pi^0 \to \mathrm{inv})$, Eq. (3.35), represents a stringent constraint, as shown in Fig. 5 (right).

Finally, the $\pi^0 \to \phi_1\phi_1$ decay could also proceed at tree level via an additional interaction term in (3.11) of the form $\delta\mathcal{L} = \lambda' m_S \phi_2 \phi_1^2$. Whereas, contrary to Model 2, λ' plays no role in the $K \to \pi\phi_1$ decays per se, it is potentially dangerous for the invisible pion decay. In the absence of a UV completion we may choose its initial value to be sufficiently small (zero in practice) to pass the constraint.

3.4.2 $\phi_1 - \pi^0$ mixing

The ϕ_i mix with light pseudoscalars through the $g_{qq'}^{(i)}$ couplings, Eq. (3.1). The $\phi_1 - \pi^0$ part of the mass matrix to one loop receives contributions in Fig. 7, and is parametrized by the Lagrangian, $m_{\phi_2} \gg m_{\phi_1,\pi,\eta}$,

$$\mathcal{L}_{\mathrm{eff}} \supset -g_{1\pi} B_0 f \phi_1 \pi^0, \tag{3.36}$$
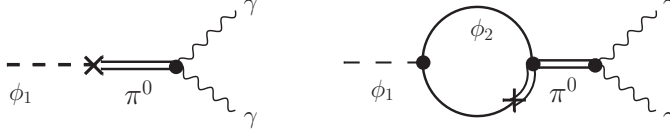
with the effective $\phi_1 - \pi^0$ coupling given by

$$\begin{aligned}
g_{1\pi} = \mathrm{Im}\, g_{dd}^{(1)} + \frac{1}{8\pi^2}\left(\frac{\lambda m_S B_0}{m_{\phi_2}^2}\right)&\left\{ \mathrm{Im}\, g_{dd}^{(2)}\, \mathrm{Re}\, g_{dd}^{(2)} L(m_\pi) \right. \\
&\left. + \frac{1}{3}\left(\mathrm{Im}\, g_{dd}^{(2)} - 2\,\mathrm{Im}\, g_{ss}^{(2)}\right)\mathrm{Re}\, g_{dd}^{(2)} L(m_\eta) + \left(\bar{g}_{ds}^{(2)}\hat{g}_{sd}^{(2)} + \mathrm{h.c.}\right)L(m_K)\right\},
\end{aligned} \tag{3.37}$$

where we have exceptionally kept the $g_{ds}^{(2)}$-terms since they are leading in BM2. The first term is due to tree level mixing, see Fig. 7 (left), the second term are the one loop corrections due to diagram in Fig. 7 (right). The loop function $L(m_X) \equiv -m_{\phi_2}^2 C_0(0, 0, 0, m_X^2, m_{\phi_2}^2, m_{\phi_2}^2)$ is normalized such that $L(m_X) \to 1$ for $m_{\phi_2} \gg m_X$. In the following we will take for simplicity this limit, which provides a reasonable approximation for the parameter region of
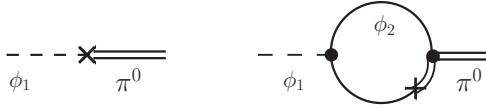
Figure 7. The leading order and one loop induced $\phi_1 - \pi^0$ mixing.

Figure 8. CP violating contributions to $\phi_1 \to \gamma\gamma$, matching onto the coupling $g_{1\gamma\gamma}$.

interest, since $L_\pi \simeq 0.8, L_{K,\eta} \simeq 0.4$ for $m_{\phi_2} = 400$ MeV. In the two benchmarks (3.30), (3.31), the effective $\phi_1 - \pi^0$ couplings are

$$\textbf{BM 1}: \qquad g_{1\pi}^{\text{BM1}} = 2.3 \times 10^{-8} \left(\frac{g_{dd}}{10^{-3}} \right)^2 \left(\frac{\text{GeV}}{m_{\phi_2}} \right)^2 , \qquad (3.38)$$

$$\textbf{BM 2}: \qquad g_{1\pi}^{\text{BM2}} = 0 . \qquad (3.39)$$

In BM2 there is no $\phi_1 - \pi^0$ mixing ϕ_1 is a pure scalar and parity is conserved.

Working in the mass insertion approximation for the off-diagonal mass term, Eq. (3.36), the $\phi_1 - \pi^0$ mixing angle, $s_\theta \equiv \sin\theta \approx \theta$, between the interaction states ϕ_1 and the mass eigenstate $\phi_1' \approx \phi_1 - s_\theta \pi^0$ is

$$s_\theta = \frac{B_0 f}{m_\pi^2 - m_{\phi_1}^2} g_{1\pi} . \qquad (3.40)$$

Note that this expression for the mixing angle is only valid for m_{ϕ_1} sufficiently far away from m_π. For the two benchmarks, we have

$$\textbf{BM 1}: \qquad s_\theta^{\text{BM1}} = 3.0 \times 10^{-7} \left(\frac{g_{dd}}{10^{-3}} \right)^2 \left(\frac{\text{GeV}}{m_{\phi_2}} \right)^2 , \qquad (3.41)$$

$$\textbf{BM 2}: \qquad s_\theta^{\text{BM2}} = 0 . \qquad (3.42)$$

The $\phi_1 - \pi^0$ mixing is thus very small in most of the viable parameter space, justifying the use of the mass insertion approximation.

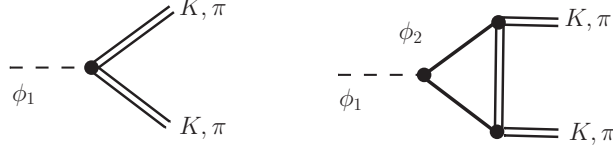### 3.4.3   Couplings of ϕ_1 to photons

The dominant decay channel of ϕ_1 is to two photons. In the limit $m_{\phi_1} \ll m_\pi$ the interactions with two photons are described by the effective Lagrangian

$$\mathcal{L}_{\text{eff}} \supset -\frac{1}{8} g_{1\gamma\gamma} \phi_1 F^{\mu\nu} F^{\rho\sigma} \epsilon_{\mu\nu\rho\sigma} - \frac{1}{4} h_{1\gamma\gamma} \phi_1 F^{\mu\nu} F_{\mu\nu} . \qquad (3.43)$$

The dominant contribution to the CP violating coupling $g_{1\gamma\gamma}$ is from the π^0 anomaly term
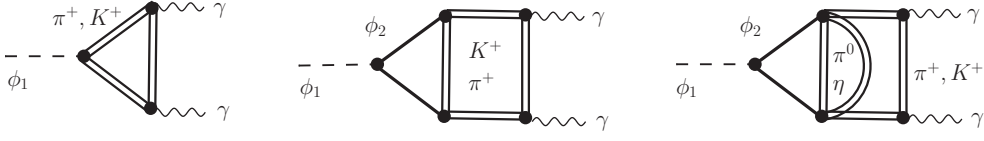
Figure 9. CP conserving contributions to $\phi_1 \to \gamma\gamma$, matching onto the coupling $h_{1\gamma\gamma}$.

Figure 10. Tree level and one loop contributions matching onto the effective couplings $g_{1\pi\pi}/g_{1KK}$.

via the $\phi_1 - \pi^0$ mixing, see Fig. 8. Working in the mass insertion approximation for the off-diagonal mass term, Eq. (3.36), gives

$$g_{1\gamma\gamma} = s_\theta \frac{\sqrt{2}\alpha}{\pi f_\pi} \approx g_{1\pi} \frac{6.2 \times 10^{-3}\,\text{GeV}}{m_\pi^2 - m_{\phi_1}^2} \xrightarrow{m_{\phi_1} \ll m_\pi} g_{1\pi}\,0.34\text{GeV}^{-1}\,, \qquad (3.44)$$

with $g_{1\pi}$ given in (3.37).

The CP conserving $h_{1\gamma\gamma}$ coupling receives the first relevant contributions from radiative corrections with K^+ and π^+ running in the loop cf. Fig. 9. For our benchmarks the first nonzero contributions arises at two loops, while for BM2 the numerically most important contribution arises at three loops

$$h_{1\gamma\gamma} = h_{1\gamma\gamma}^{1+2\,\text{loop}} + h_{1\gamma\gamma}^{3\,\text{loop}}\,. \qquad (3.45)$$

In the $m_{\phi_2} \gg m_K$ ($m_\pi \gg m_{\phi_1}$ by assumption) limit the one and two loop contributions, in Fig. 9, assume the form

$$h_{1\gamma\gamma}^{1+2\,\text{loop}} = \frac{\alpha}{12\pi}\left(\frac{g_{1\pi\pi}}{m_\pi^2} + \frac{g_{1KK}}{m_K^2}\right)\,, \qquad (3.46)$$

whereas the effective couplings of ϕ_1, $\mathcal{L}_{\text{eff}} \supset \phi_1\left(g_{1\pi\pi}\pi^+\pi^- + g_{1KK}K^+K^-\right)$, to two light charged mesons evaluate to

$$g_{1\pi\pi} = B_0\left[\text{Re}\,g_{dd}^{(1)} + \frac{\lambda B_0 m_S}{8\pi^2 m_{\phi_2}^2}\left((\text{Re}\,g_{dd}^{(2)})^2 + |\bar{g}_{sd}^{(2)}|^2\right)\right]\,, \qquad (3.47)$$

and $g_{1KK} = g_{1\pi\pi}|_{dd \to ss}$. The first term in (3.47) is the tree level term from (3.12), see Fig. 10 (left). In both benchmarks, BM1 and BM2, this contribution was set to zero. The second term in (3.47) is the one loop correction, see Fig. 10 (right). We kept the flavor violating contribution proportional to $\bar{g}_{sd}$ even though it is numerically negligible.

For the three loop contribution to $h_{1\gamma\gamma}$ we resort to a NDA estimate, still in the $m_{\phi_2} \gg m_K$ limit,

$$h_{1\gamma\gamma}^{3\,\text{loop}} \approx \frac{\alpha}{4\pi}\frac{\lambda m_S}{(16\pi^2)^2}\left(\frac{B_0}{f m_{\phi_2}}\right)^2\left[\left(\text{Im}\,g_{dd}^{(2)}\right)^2 + \mathcal{O}(1) \times (\text{Im}\,g_{ss}^{(2)})^2 + \mathcal{O}(1) \times (\text{Im}\,g_{dd}^{(2)})(\text{Im}\,g_{ss}^{(2)})\right],$$

where the $\mathcal{O}(1)$ factors are not displayed.

Finally we are in a position to assemble the results for the benchmarks. Using $g_{sd} \ll g_{dd}$, the ϕ_1–photon couplings evaluate to

$$\textbf{BM1}: \quad g_{1\gamma\gamma}^{\text{BM1}} \simeq \frac{7.7 \times 10^{-9}}{\text{GeV}} \left(\frac{g_{dd}}{10^{-3}}\right)^2 \left(\frac{\text{GeV}}{m_{\phi_2}}\right)^2 ,$$
$$h_{1\gamma\gamma}^{\text{BM1}} \simeq \frac{4.8 \times 10^{-10}}{\text{GeV}} \left(\frac{g_{dd}}{10^{-3}}\right)^2 \left(\frac{\text{GeV}}{m_{\phi_2}}\right)^2 , \tag{3.48}$$

in BM1, while for BM2 they turn out to be

$$\textbf{BM2}: \quad g_{1\gamma\gamma}^{\text{BM2}} = 0 ,$$
$$h_{1\gamma\gamma}^{\text{BM2}} \sim \frac{2 \times 10^{-14}}{\text{GeV}} \left(\frac{g_{dd}}{3 \times 10^{-5}}\right)^2 \left(\frac{\text{GeV}}{m_{\phi_2}}\right)^2 , \tag{3.49}$$

and we remind the reader that $\lambda m_S = 1$ GeV for reference. The $g_{1\gamma\gamma}$ coupling vanishes in BM2 since ϕ_1 is a parity even scalar in that benchmark. The value quoted for $h_{1\gamma\gamma}^{\text{BM2}}$ is the NDA estimate of the flavor conserving 3 loop contribution. For representative values of g_{dd} in the two benchmarks we used the values in Figs. 5 and Fig. 6 for BM1 and BM2, respectively.

The above couplings of ϕ_1 to photons are sufficiently small that for both benchmarks the ϕ_1 is stable on collider scales. More concretely, the $\phi_1 \to \gamma\gamma$ partial decay width is given by

$$\Gamma_{1\gamma\gamma} = \frac{1}{64\pi}\left(g_{1\gamma\gamma}^2 + h_{1\gamma\gamma}^2\right)m_{\phi_1}^3 , \tag{3.50}$$

and this translates to

$$\textbf{BM1}: \quad c\tau_{1\gamma\gamma}^{\text{BM1}} = 7 \times 10^{11}\,\text{m} \left(\frac{\text{MeV}}{m_{\phi_1}}\right)^3 \left(\frac{10^{-3}}{g_{dd}}\right)^4 \left(\frac{m_{\phi_2}}{\text{GeV}}\right)^4 , \tag{3.51}$$

$$\textbf{BM2}: \quad c\tau_{1\gamma\gamma}^{\text{BM2}} \sim 10^{23}\,\text{m} \left(\frac{\text{MeV}}{m_{\phi_1}}\right)^3 \left(\frac{3 \times 10^{-5}}{g_{dd}}\right)^4 \left(\frac{m_{\phi_2}}{\text{GeV}}\right)^4 , \tag{3.52}$$

such that ϕ_1 is stable on solar to cosmological timescales. For such small couplings the laboratory constraints from, e.g., $\pi^+ \to \phi_1 e^+\nu$ decays [37] are irrelevant, whereas astrophysical and cosmological constraints are important (cf. figure 1 in Ref. [38]) and further discussed in Section 3.4.5.

3.4.4 Couplings of ϕ_1 to nucleons

The couplings of ϕ_1 to protons and neutrons are tree-level and loop-level induced by $g_{dd}^{(1)}$ and $g_{dd}^{(2)}$ respectively, cf. Fig. 11. One can use Heavy Baryon Chiral Perturbation Theory (HBChPT) [39] to organize different contributions. We only keep only the leading terms which are (in relativistic notation)

$$\mathcal{L} = \frac{g_A}{f}(\bar{N}\gamma^\mu\gamma_5 t^a N)\partial_\mu\pi^a + \sum_i (\bar{N}Y_i^N N)\phi_i + \cdots , \tag{3.53}$$

with $t^a = \sigma^a/2$, $a = 1, 2, 3$ and σ^a are Pauli matrices, $N = (p, n)$ the isospin doublet of nucleons, and

$$Y_i^N = \begin{pmatrix} \sum_q \text{Re}(g_{qq}^{(i)})\sigma_q^p/m_q & 0 \\ 0 & \sum_q \text{Re}(g_{qq}^{(i)})\sigma_q^n/m_q \end{pmatrix}, \tag{3.54}$$

the coupling between ϕ_i and nucleons with summation over $q = d, s$ (by assumption the couplings of $\phi_{1,2}$ to up quarks are zero). For the matrix elements of the scalar current, $\sigma_q^N \bar{u}_N u_N = \langle N|m_q \bar{q}q|N\rangle$ we use the values from [40], $\sigma_d^p = (32 \pm 10)$ MeV, $\sigma_d^n = (36 \pm 10)$ MeV, $\sigma_s^p = \sigma_s^n = (41.3 \pm 7.7)$ MeV, along with the quark masses at $\mu = 2$ GeV, $m_d = 4.67(33)$ MeV, $m_s = 93(8)$ MeV, while $g_A = 1.2723(23)$ [27].

In the heavy ϕ_2 limit the following effective Lagrangian

$$\mathcal{L}_{\text{eff}} = g_{1NN} m_N \phi_1 (\bar{N}N) + 2\tilde{g}_{1NN} m_N \phi_1 (\bar{N}i\gamma_5 t^3 N), \tag{3.55}$$

provides a good description of the ϕ_1-nucleon system. Assuming $m_{\phi_2,N} \gg m_{\phi_1}$, the diagrams in Fig. 11, evaluate to

$$g_{1NN} = \frac{1}{m_N}\left[Y_1^N - \frac{\lambda m_S}{8\pi^2 m_N}\left\{ (Y_2^N)^2 F(r) - \left(g_A \text{Im}\, g_{dd}^{(2)} \frac{B_0}{m_N}\right)^2 \tilde{F}(r)\right\}\right], \tag{3.56}$$

$$\tilde{g}_{1NN} = \frac{g_A B_0}{m_\pi^2 - m_{\phi_1}^2}\left[\text{Im}\, g_{dd}^{(1)} + \frac{\lambda m_S}{12\pi^2}\left(\frac{B_0}{m_{\phi_2}^2}\right)\left(2\,\text{Im}\, g_{dd}^{(2)} - \text{Im}\, g_{ss}^{(2)}\right)\text{Re}\, g_{dd}^{(2)}\right], \tag{3.57}$$

where Y_1^N stands for the nucleon-nucleon entries in (3.54). In the $\tilde{F}(r)$ term in (3.56) we in addition assumed the $m_\pi \gg m_{\phi_1}$ limit. The real-valued loop functions $F(r)$, $\tilde{F}(r)$, with $r = m_{\phi_2}^2/m_N^2$, are given by[6]

$$F(r) = \frac{(r-3)}{2}\log r - 1 + (1-r)\sqrt{1-4/r}\,\log\left[\frac{1}{2}\left(\sqrt{r-4} + \sqrt{r}\right)\right], \tag{3.58}$$

$$\tilde{F}(r) = \frac{1}{r^2\sqrt{1-4/r}}\log\left[\frac{1}{2}\left(\sqrt{r-4} + \sqrt{r}\right)\right]. \tag{3.59}$$

In the limit $m_{\phi_2} \gg m_N$ we have $F(r) \to -3/(2r)$, $\tilde{F}(r) \to \ln r/(2r^2)$. For $m_{\phi_2} \in [0.5, 1.5]$ GeV the loop functions take values in the intervals $F(r) \in [-2.7, -0.46]$, $\tilde{F}(r) \in [4.5, 0.13]$. The first term in (3.56) is due to the 1st diagram, while the one loop corrections are due to the 2nd and 5rd diagram in Fig. 11. For the pseudoscalar coupling to nucleons, $\tilde{g}_{1NN}$, we keep the pion exchange term (dropping the η-exchange) in the 4th and the 5th diagram in Fig. 11 resulting in the tree level and one loop terms in (3.57). To simplify the expressions we show the one loop contribution in (3.57) only in the heavy m_{ϕ_2} limit.

Numerically, we have for BM1, setting $m_{\phi_2} = 1$ GeV,

$$g_{1NN}^{\text{BM1}} \simeq 3.5(4.3) \times 10^{-7}\,\text{GeV}^{-1}\left(\frac{g_{dd}}{10^{-3}}\right)^2, \tag{3.60}$$

---

[6]It is noted that the 3rd diagram, in Fig. 11, does not introduce any infrared (IR) divergences in the limit $m_\pi \to 0$. This is a consequence of the derivative couplings of pions, cf. Eq. (3.53). We note in passing that for a double insertion of this interaction term one cannot use the naive EOM and replace $g_A(\bar{N}\gamma^\mu\gamma_5 t^a N)\partial_\mu\pi^a \to -2m_N g_A \bar{N}\gamma_5 t^a N\pi^a$. For a concise technical discussion we refer the reader to Ref. [41]. Use of the naive EOM leads to the IR divergence that is linked to the absence of the derivative coupling in that case. The same applies to the single insertion of the g_A-term in 4th and 5th diagram.
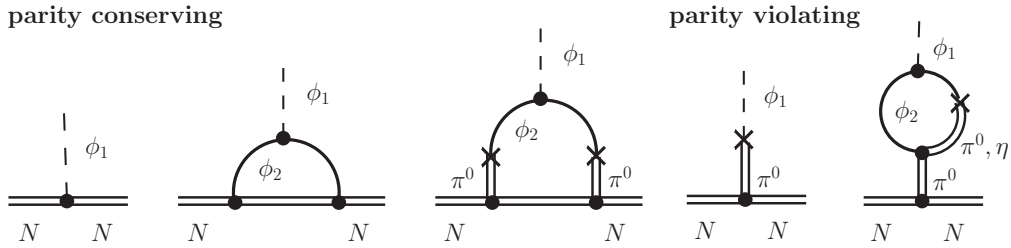
Figure 11. The leading order and one loop induced ϕ_1-couplings to nucleons grouped into parity conserving coupling g_{1NN} (even in g_A) and parity violating coupling $\tilde{g}_{1NN}$ in (3.56) (odd in g_A). The 3rd diagram is the only non-vanishing contribution to g_{1NN} in BM2.
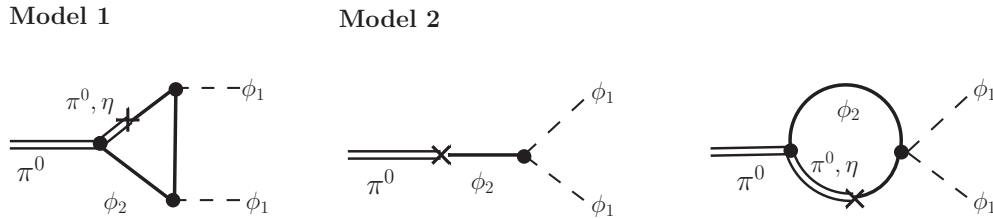
Figure 12. Diagrams for the invisible pion decay, $\pi^0 \to \phi_1\phi_1$, in Model 1 (left) and Model 2 (middle and right). The diagram for Model 3 are analogous to Model 2 with the difference that the graph on the right needs an extra ψ_2 propagator as in Fig. 18.

$$\tilde{g}_{1NN}^{\text{BM1}} \simeq \quad 4 \times 10^{-6}\,\text{GeV}^{-1} \left(\frac{g_{dd}}{10^{-3}}\right)^2 , \tag{3.61}$$

where the g_{1NN}^{BM1} central value refers to protons (neutrons), while for BM2,

$$g_{1NN}^{\text{BM2}} \simeq 8 \times 10^{-11}\,\text{GeV}^{-1} \left(\frac{g_{dd}}{3 \times 10^{-5}}\right)^2 , \tag{3.62}$$

$$\tilde{g}_{1NN}^{\text{BM2}} = 0 . \tag{3.63}$$

Below we analyse the combined constraints from the previous two subsections.

3.4.5 Combined analysis of ϕ_1-constraints

The most important constraint on the ϕ_1-couplings comes from the neutrino burst duration observed in the supernova SN1987A. The interactions of ϕ_1 with matter inside an exploding supernova are dominated by its couplings to nucleons. For $m_{\phi_1} = 1$ MeV, used in our benchmarks, the SN1987A observations exclude $g_{1NN}^{\text{eff}} \equiv (\tilde{g}_{1NN}^2 + (3/2)g_{1NN}^2)^{1/2}$ in the range $7 \cdot 10^{-10}\,\text{GeV}^{-1} \lesssim g_{1NN}^{\text{eff}} \lesssim 4 \cdot 10^{-6}\,\text{GeV}^{-1}$ [42]. For larger values of g_{1NN}^{eff} the ϕ_1 gets trapped inside the proto-neutron star (PNS) and does not contribute to the cooling. This is the case for BM1, see Eqs. (3.60), (3.61). For smaller values of g_{1NN}^{eff} the emission of ϕ_1 is suppressed sufficiently that it again does not contribute appreciably to the cooling of PNS. BM2 falls in this regime, see Eqs. (3.62), (3.63).

The photon couplings of ϕ_1 are less relevant for SN1987A since the Primakoff emission of ϕ_1 is always subdominant relative to the emission of ϕ_1 in nucleon-nucleon scattering.
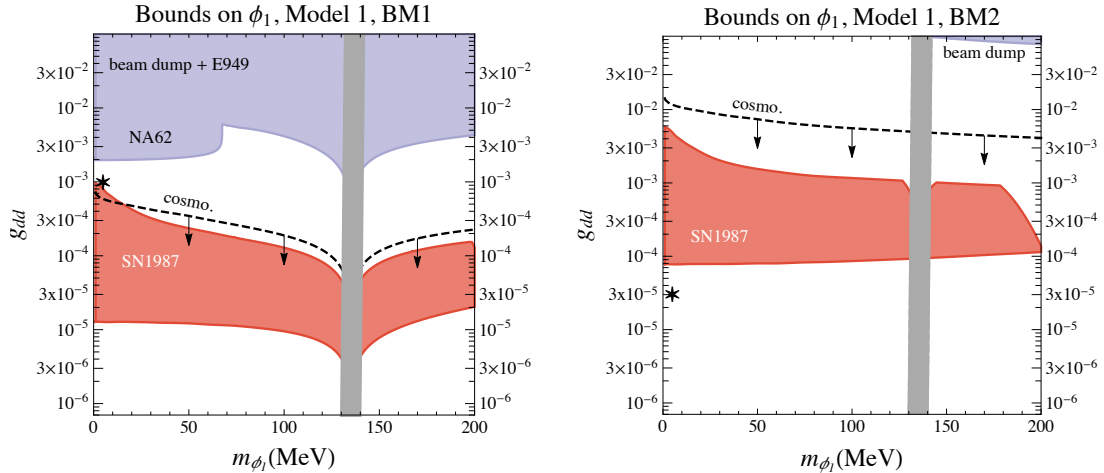
Figure 13. The constraints on the g_{dd} coupling in BM1 (left) and BM2 (right) due to couplings of ϕ_1 to photons and nucleons as a function of the ϕ_1 mass. The purple regions are excluded by beam dump searches, E949 ($K^+ \to \pi^+ X$) and NA62($\pi^0 \to$ inv), the red region by SN1987, while the dashed line shows the upper bound from cosmology in the absence of any other light states or ϕ_1-couplings. The star denotes the values of g_{dd} and m_{ϕ_1} in Fig. 5 (Fig. 6) for BM1 (BM2). The region around $m_{\phi_1} \simeq m_{\pi^0}$ is masked out (gray region).

This is best illustrated by the fact that SN1987A would exclude the range $10^{-8}\text{GeV}^{-1} \lesssim g_{1\gamma\gamma}, h_{1\gamma\gamma} \lesssim 10^{-5}\text{GeV}^{-1}$, if ϕ_1 were to coupled to photons only. The induced couplings of ϕ_1 to photons are at the lower edge of this range for BM1 and well below for BM2, cf. Eqs. (3.48) and (3.49) respectively. This should be contrasted with nucleon couplings which for BM1 traps ϕ_1 inside the PNS as it is above and not below the exclusion window.

The constraints from the SN1987A neutrino burst duration are shown for a range of ϕ_1 masses for benchmarks BM1 and BM2 in Fig. 13 (left) and (right) as red regions, respectively. According to the analysis of Ref. [42], the bounds are relevant all the way up to $m_{\phi_1} \lesssim 300$ MeV, though we truncate the plots at 200 MeV. These bounds may however depend on the details of the SN1987A explosion, and may even be absent if this was due to a collapse-induced thermonuclear explosion [43].

In addition, Fig. 13 shows with purple shading the constraints from beam dump experiments (we use the combined limit as quoted in [42]), and from the invisible pion decay by NA62 [8]. The $\phi_1 - \pi^0$ mixing angle s_θ needs to be smaller than about 2×10^{-5} in order to satisfy the $K^+ \to \pi^+ X$ constraints from E949 [29] and NA62 [8]. This imposes a constraint on g_{dd} that is comparable but slightly less stringent than the beam dump limit. The upper bound from cosmology, i.e., the impact of ϕ_1 decays on big bang nucleosynthesis and distortions of cosmic microwave background, are shown with a dashed line [44]. This bound is very sensitive to the details of the model. For instance, if the ϕ_1 decays predominantly to neutrinos these bounds would be drastically modified and thus potentially irrelevant.
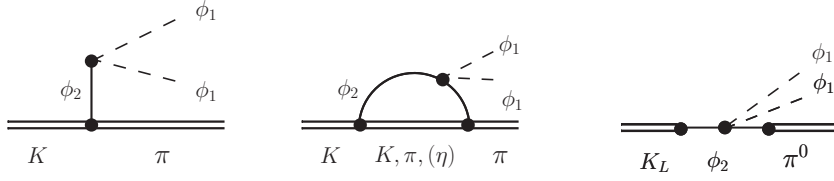
Figure 14. The diagrams inducing the $K \to \pi\phi_1\phi_1$ decays in Model 2, with the matrix elements shown in Eqs. (4.3) and (4.4). The 3rd diagram violates the GN bound.

4 Model 2 - scalar model leading to the three-body kaon decays

Model 2 has the same field content as Model 1, except that we impose a Z_2 symmetry under which the scalar ϕ_1 is odd, $\phi_1 \to -\phi_1$. The relevant terms in the Lagrangian are

$$\mathcal{L} \supset g_{qq'}^{(2)}(\bar{q}_L q'_R)\phi_2 + \text{h.c.} + \lambda_4 \phi_2^2 \phi_1^2 + \lambda' m_S \phi_2 \phi_1^2 + \lambda'' m_S \phi_2^3 + \cdots . \tag{4.1}$$

Note that the coupling $(\bar{q}_L q'_R)\phi_1$ is forbidden by the Z_2-parity. Because of the Z_2 parity the ϕ_1 always appears in pairs in the final state and we thus focus on the $K \to \pi\phi_1\phi_1$ transitions with leading diagrams shown in Fig. 14.

The 1st diagram in Fig. 14, proportional to the trilinear coupling λ', gives the same contribution to both $K^+ \to \pi^+\phi_1\phi_1$ and $K^0 \to \pi^0\phi_1\phi_1$ transitions in accordance with isospin. Since we are interested in violations of the GN bound, we impose the hierarchy

$$\lambda', \lambda'' \ll \lambda_4 , \tag{4.2}$$

and assume $m_S = \mathcal{O}(m_K)$. For simplicity we further assume that $\phi_{1,2}$ do not have vevs, or that they are negligibly small (cf. related discussion for Model 1 in Section 3).

Keeping the leading diagrams in the λ' and $\lambda_4 g_{dd}^{(2)}$ expansion, i.e., the diagrams in Fig. 14, the $K_L \to \pi^0\phi_1\phi_1$ decay amplitude reads

$$\mathcal{M}(K_L \to \pi^0\phi_1\phi_1)_{\text{NP}} = i\Big\{ 4\,\text{Im}\,\hat{g}_{sd}^{(2)}\,\text{Im}\,g_{dd}^{(2)}\lambda_4\Delta_{\phi_2}(m_K^2)\Delta_{\phi_2}(m_\pi^2)B_0 f_K f_\pi$$
$$- 2\,\text{Im}\,\bar{g}_{sd}^{(2)}\lambda' m_S\Delta_{\phi_2}(q^2) - \frac{\text{Im}\,\bar{g}_{sd}^{(2)}}{4\pi^2}\lambda_4\mathcal{F}_L^{(2)}(\tilde{I})B_0\Big\}B_0 , \tag{4.3}$$

with $\mathcal{F}_L^{(2)}$ given in (3.15), while the $K^+ \to \pi^+\phi_1\phi_1$ decay amplitude is

$$\mathcal{M}(K^+ \to \pi^+\phi_1\phi_1)_{\text{NP}} = \Big\{ 2\bar{g}_{sd}^{(2)}\lambda' m_S\Delta_{\phi_2}(q^2) + \frac{\bar{g}_{sd}^{(2)}}{4\pi^2}\lambda_4 B_0\mathcal{F}_+^{(2)}(\tilde{I})\Big\}B_0 , \tag{4.4}$$

with $\mathcal{F}_+^{(2)}$ defined in (3.16), $\tilde{I}(m_M) = C_0(m_K^2, q^2, m_\pi^2, m_M^2, m_{\phi_2}^2, m_{\phi_2}^2)$, and $q^2 = (p_1 + p_2)^2$ is the invariant mass squared of the $\phi_1\phi_1$ final state system. As for Model 1, $f^2 \to f_\pi f_K/2$ in order to account for the main SU(3) breaking effect.

The structure of the two decay amplitudes is reminiscent of the results in Model 1 in Eqs. (3.13), (3.14). The main difference is that there is no direct coupling of ϕ_1 to quarks

due to the Z_2 symmetry. The $\phi_1\phi_1$ pair couples to $d \to s$ current instead through the off-shell tree level exchange of ϕ_2, see the 1st diagram in Fig. 14. This leads to isospin symmetric contributions to $K^+ \to \pi^+\phi_1\phi_1$ and $K_L \to \pi^0\phi_1\phi_1$, proportional to the trilinear λ' coupling. Hence, in the $\lambda' \to 0$ limit, the $K^+ \to \pi^+\phi_1\phi_1$ transition only receives loop contributions, and the GN bound is maximally violated. Note that λ' cannot be arbitrarily small, since it is generated at one loop through ϕ_2 loop, $\lambda' \sim \lambda_4\lambda''/(16\pi^2)$, and at two loops with ϕ_2 and π^0, η running in the loop: $\lambda' \sim \lambda_4(g_{dd}^{(2)})^3/(16\pi^2)^2$. For our benchmarks this gives a vanishingly small λ' and thus this contribution can be safely ignored in our analysis provided the bare value of λ', λ'' are set to zero. In this limit the first isospin conserving contribution is at one loop due to the 2nd diagram in Fig. 14. The GN-violating contribution instead arises at tree level, see the 3rd diagram in Fig. 14 and the first term in (4.3).

The total rate of $K_L \to \pi^0\phi_1\phi_1$ adds coherently to the SM $K_L \to \pi^0\nu\bar{\nu}$ rate. The differential rate for $K_L \to \pi^0\phi_1\phi_1$ is given by

$$\frac{d\Gamma}{dE_\pi} = \frac{|\mathcal{M}|^2}{128\pi^3 m_K}p_\pi\beta_{\phi_1} \ , \tag{4.5}$$

where $p_\pi = \sqrt{E_\pi^2 - m_\pi^2}$ and $E_\pi = (m_K^2 + m_\pi^2 - q^2)/(2m_K)$ are the pion's momentum and energy in the K_L rest frame, while $\beta_{\phi_1} = (1 - 4m_{\phi_1}^2/q^2)^{1/2}$.

4.1 Benchmarks for Model 2

The bounds from $K^0 - \bar{K}^0$ mixing on flavor violating ϕ_2-coupling $\hat{g}_{sd}^{(2)}$ are exactly the same as for Model 1, Section 3.2. To illustrate the available parameter space we therefore use the same two benchmarks for the ϕ_2-couplings, Eqs. (3.30), (3.31), with results shown in Figs. 15, 16. In both cases we set $\lambda_4 = 1$ and all the other couplings, apart from the ones in Eqs. (3.30, 3.31), to zero (including λ'). In summary, the two benchmarks for Model 2 are thus

Model 2, BM 1 :   Eq. (3.30) and $m_{\phi_1} = 100$ MeV, $\lambda_4 = 1$, $\lambda' = \lambda'' = 0$, (4.6)

Model 2, BM 2 :   Eq. (3.31) and $m_{\phi_1} = 100$ MeV, $\lambda_4 = 1$, $\lambda' = \lambda'' = 0$, (4.7)

while m_{ϕ_2} is kept as a free parameter. The results in Figs. 15, 16 are fairly independent of the ϕ_1 mass as long as it is taken to be small, $m_{\phi_1} \ll m_K$, and thus does not modify the final phase space. The choice of benchmark value $m_{\phi_1} = 100$ MeV is driven by the constraints of the invisible pion decays, see Section 4.2. BM1 and BM2 thus have three free parameters: g_{dd}, g_{sd} and m_{ϕ_2}.

BM1, shown in Fig. 15, has a well restricted $\{g_{sd}, m_{\phi_2}\}$ parameter space, since the tree level exchanges of ϕ_2 contributes a new CP violating source in $K^0 - \bar{K}^0$ mixing. This then restricts g_{sd} to be below the hatched region in Fig. 15 (right), see also Eq. (3.29). However, large enhancements of $\mathrm{Br}(K_L \to \pi^0 + \mathrm{inv})$ over $\mathrm{Br}(K^+ \to \pi^+ + \mathrm{inv})$ are still possible in significant parts of the parameter space. For instance, setting $g_{dd} = 5 \cdot 10^{-2}$, the KOTO upper bound $\mathrm{Br}(K_L \to \pi^0\nu\bar{\nu})_{\mathrm{exp}} < 3.0 \times 10^{-9}$ [9] (red region in Fig. 15) are obtained for $g_{sd} \lesssim \mathcal{O}(10^{-9})$ and $m_{\phi_2} \lesssim \mathcal{O}(1 \text{ GeV})$. Fig. 15 (left) shows that in the relevant region of parameter space the deviations in $\mathrm{Br}(K^+ \to \pi^+ + \mathrm{inv})$ from the SM prediction are
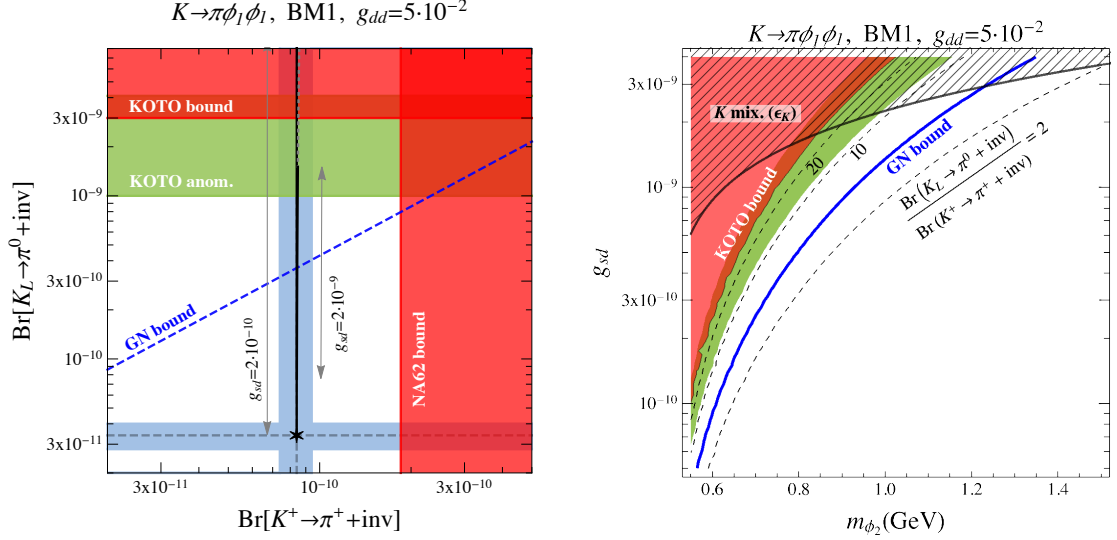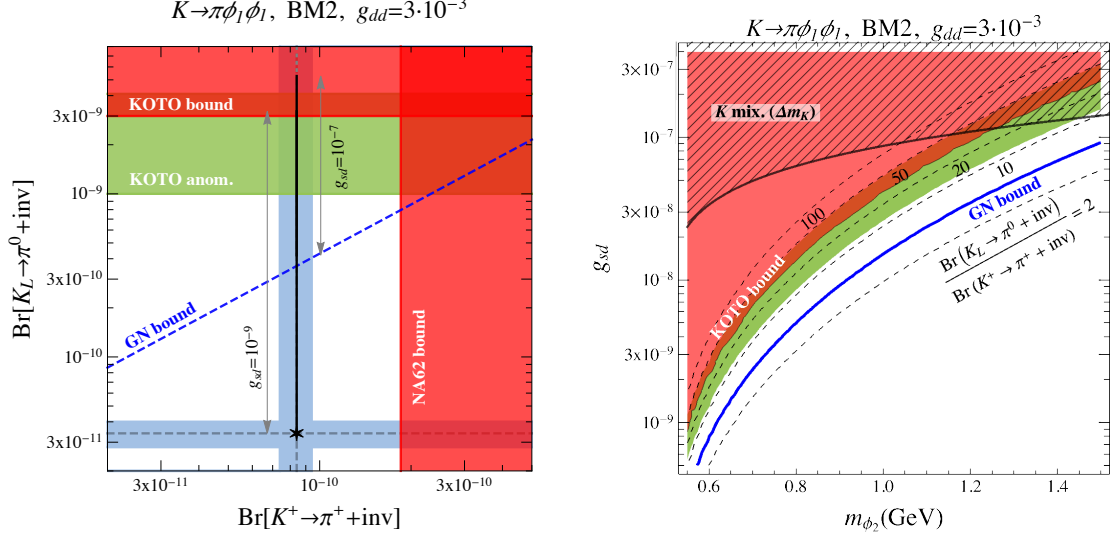
Figure 15. The parameter space for Model 2, BM1, Eq. (4.6). The color coding is the same as in Fig. 5. In the predictions for $\mathrm{Br}(K^+ \to \pi^+ + \mathrm{inv})$, $\mathrm{Br}(K_L \to \pi^0 + \mathrm{inv})$ on the left plot (black lines) we vary $m_{\phi_2} \in [0.55, 1.5]$ GeV for two values of $g_{sd} = 2 \times 10^{-10}, 2 \times 10^{-9}$.

negligible, while $\mathrm{Br}(K_L \to \pi^0 + \mathrm{inv})$ can be enhanced well above the GN bound (blue line). For illustration we vary $m_{\phi_2} \in [0.55, 1.5]$ GeV, the same range as is shown in Fig. 15 (right), fix $g_{dd} = 5 \cdot 10^{-2}$ and show predictions for two choices of $g_{sd} = 2 \cdot 10^{-10}, 2 \cdot 10^{-9}$ (black lines). The resulting range in $\mathrm{Br}(K_L \to \pi^0 + \mathrm{inv})$ is denoted with arrows. For $g_{sd} = 2 \cdot 10^{-9}$ the ϵ_K bound is reached, and the exclusion range is shown with gray dotted lines. For both choices of g_{sd} the enhancements can easily be in the range of the KOTO anomaly (green band) without violating any other bounds.

For BM2 the allowed $\{g_{sd}, m_{\phi_2}\}$ parameter space is much larger, since in this case ϕ_2 exchanges only induce CP conserving contributions to $K^0 - \bar{K}^0$ mixing. This gives the bound in (3.24), denoted in Fig. 16 (right) with the hatched region. Very large violations of the GN bound (blue line) are thus possible without violating $K^0 - \bar{K}^0$ mixing constraints. For instance, for $g_{dd} = 3 \cdot 10^{-3}$ the KOTO upper bound is reached for $g_{sd} \sim \mathrm{few} \times 10^{-8}$ and $m_{\phi_2} \sim 1$ GeV. Fig. 16 (left) shows predictions for $\mathrm{Br}(K^+ \to \pi^+ + \mathrm{inv})$, $\mathrm{Br}(K_L \to \pi^0 + \mathrm{inv})$, for two choices of $g_{sd} = 10^{-9}, 10^{-7}$ (black lines, gray dotted line excluded by $K^0 - \bar{K}^0$ mixing) when varying $m_{\phi_2} \in [0.55, 1.5]$ GeV, setting $g_{dd} = 3 \cdot 10^{-3}$. The deviations in $\mathrm{Br}(K^+ \to \pi^+ + \mathrm{inv}) = 1.0 \cdot 10^{-8}$ vanish in BM2, while over a large region of $\{g_{dd}, g_{sd}, m_{\phi_2}\}$ the KOTO upper limits on $\mathrm{Br}(K_L \to \pi^0 + \mathrm{inv})$ are saturated, while avoiding any other constraints.

Figure 16. The preferred parameter space for Model 2, BM2. The color coding is the same as in Fig. 15. For the model predictions (black lines) in the left panel we set $g_{sd} = 10^{-9}, 10^{-7}$ and vary $m_{\phi_2} \in [0.55, 1.5]$ GeV.

4.2 Constraints on the ϕ_1-couplings

The most stringent constraints on the couplings of ϕ_1 to quarks are due to the invisible π^0 decay. In the $m_{\phi_2} \gg m_\pi$ limit, the $\pi^0 \to \phi_1 \phi_1$ decay amplitude is given by,

$$\mathcal{M}(\pi^0 \to \phi_1 \phi_1) = \frac{B_0 f}{m_{\phi_2}^2} \left[2\lambda' m_S \operatorname{Im} g_{dd}^{(2)} + \frac{\lambda_4 B_0}{6\pi^2} \operatorname{Re} g_{dd}^{(2)} \left(2 \operatorname{Im} g_{dd}^{(2)} - \operatorname{Im} g_{ss}^{(2)} \right) \right], \qquad (4.8)$$

where the first term in the parenthesis originates from the tree level exchange of the ϕ_2, Fig. 12 (middle), the second from the one loop contribution shown in Fig. 12 (right).

Using Eq. (3.33) for the $\pi^0 \to \phi_1 \phi_1$ partial decay width, the corresponding branching ratio in the $m_{\phi_1} \ll m_\pi \ll m_{\phi_2}$ limit are, setting $g_{ss}^{(2)} = 0$,

$$\operatorname{Br}(\pi^0 \to \phi_1 \phi_1) = \begin{cases} 3.8 \times 10^{-3} \lambda_4^2 \left(\frac{\operatorname{Re} g_{dd}^{(2)}}{3 \times 10^{-2}} \right)^2 \left(\frac{\operatorname{Im} g_{dd}^{(2)}}{3 \times 10^{-2}} \right)^2 \left(\frac{\text{GeV}}{m_{\phi_2}} \right)^4, & \text{for } \lambda' = 0, \\ 2.1 \times 10^{-7} \left(\frac{\lambda' m_S}{10^{-5} \, \text{GeV}} \right)^2 \left(\frac{\operatorname{Im} g_{dd}^{(2)}}{3 \times 10^{-2}} \right)^2 \left(\frac{\text{GeV}}{m_{\phi_2}} \right)^4, & \text{for } \lambda_4 = 0. \end{cases} \qquad (4.9)$$

These should be compared with the experimental bound $\operatorname{Br}(\pi^0 \to \phi_1 \phi_1) < 4.4 \times 10^{-9}$ [8]. For $\lambda_4 \sim \mathcal{O}(1)$, which is required for large violations of the GN bound, this excludes ϕ_1 masses $m_{\phi_1} \lesssim m_\pi/2$ for BM1. In BM2 the $\pi^0 \to \phi_1 \phi_1$ is forbidden due to parity, so that ϕ_1 can be light, as long as the parity breaking term $\lambda' m_S$ is sufficiently small.

The beam dump and SN constraints in BM1 and BM2 are very similar to the ones shown in Fig. 13 for Model 1, but with rough identification $g_{dd}|_{\text{Model 1}} \to 1/(4\pi) \times g_{dd}|_{\text{Model 2}}$ and $m_{\phi_1}|_{\text{Model 1}} \to 2m_{\phi_1}|_{\text{Model 2}}$, since the transitions now involve two ϕ_1 particles in the final state. In particular, for the choices of parameters in Figs. 15 and 16 the collider and SN constraints are presumably satisfied.
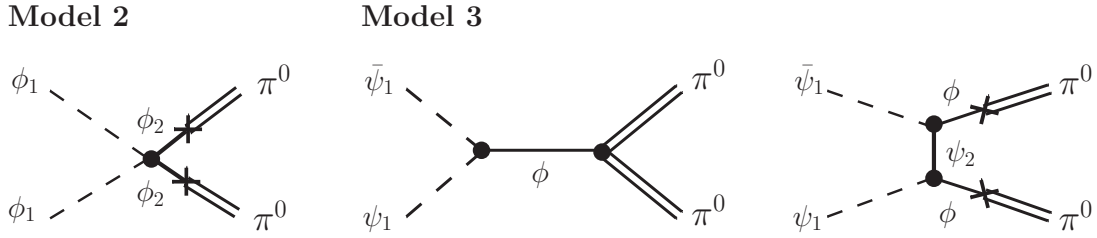
Figure 17. Graph dominating the annihilation cross section of $\phi_1\phi_1 \to \pi^0\pi^0$ and $\psi_1\bar{\psi}_1 \to \pi^0\pi^0$ in Model 2 and Model 3 respectively.

4.3 ϕ_1 as a dark matter candidate

Since ϕ_1 is odd under the Z_2-parity, it is absolutely stable and could be a dark matter (DM) candidate. If $m_{\phi_1} > m_{\pi^0}$ the $\phi_1\phi_1 \to \pi^0\pi^0$ annihilation channel is open. Below we shall see that the annihilation cross section is large enough, in part of the parameter space, such that the correct DM relic abundance is obtained. Note however, that this restricts ϕ_1 to a rather narrow mass range, $m_{\pi^0} \leq m_{\phi_1} \leq (m_{K_L} - m_{\pi^0})/2$, or numerically, $135 \text{ MeV} \lesssim m_{\phi_1} \lesssim 181$ MeV.

The annihilation cross section for $\phi_1\phi_1 \to \pi^0\pi^0$ process is dominated by the λ_4 vertex and $\phi_2 - \pi^0$-conversion, while the ϕ_2 s-channel resonance contribution is subleading, since $\lambda' \ll \lambda_4$, cf. (4.2) and Fig. 17. Assuming a non-relativistic ϕ_1, as is the case at the time of freeze-out, the leading thermally averaged cross section is given by

$$\langle \sigma v \rangle = \frac{1}{16\pi} \lambda_4^2 \big(\text{Im} \, g_{dd}^{(2)} \big)^4 \left(\frac{B_0 f_\pi}{m_{\phi_2}^2} \right)^4 \frac{p_\pi}{m_{\phi_1}^3} \, , \tag{4.10}$$

where in this approximation $p_\pi = (m_{\psi_1}^2 - m_\pi^2)^{1/2}$. Taking $m_{\phi_1} = 160$ MeV as a representative value gives

$$\langle \sigma v \rangle \simeq 3 \cdot 10^{-26} \frac{\text{cm}^3}{\text{s}} \times \lambda_4^2 \left(\frac{\text{Im} \, g_{dd}^{(2)}}{2.56 \times 10^{-2}} \right)^4 \left(\frac{1 \text{ GeV}}{m_{\phi_2}} \right)^4 , \tag{4.11}$$

which is of the right size to get the correct DM relic abundance ($3 \cdot 10^{-26} \text{cm}^3/\text{s} \approx 1 \text{ pb}$).

For $m_{\phi_1} < m_{\pi^0}$ the $\phi_1\phi_1 \to \pi^0\pi^0$ annihilation cross section is kinematically forbidden. In that case the dominant annihilation channel becomes $\phi_1\phi_1 \to \gamma\gamma$. The resulting annihilation cross section is so small, that if this were the only annihilation channel, the ϕ_1 would overclose the universe [45]. This means that ϕ_1 should also couple to other light states. For instance, ϕ_1 could annihilate into light SM particles, e.g. $\phi_1\phi_1 \to e^+e^-$ or $\phi_1\phi_1 \to \nu\bar{\nu}$. Alternatively it could annihilate away to other light dark sector particles or dark photons $\phi_1\phi_1 \to \gamma_D\gamma_D$ (if ϕ_1 was gauged under a dark $U(1)$). Since none of these couplings are related to $K \to \pi\phi_1\phi_1$ decays we do not explore the related phenomenology any further, beyond stating the obvious – that ϕ_1 could well be a thermal relic for appropriate values of these additional couplings.
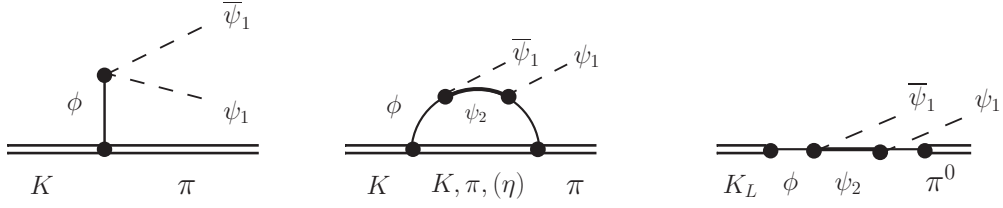
Figure 18. The $K \to \pi \psi_1 \bar{\psi}_1$ in the fermion Model 3 with contribution evaluated in Eqs. (4.3) and (5.8) respectively. The third diagram only contributes to $K_L \to \pi^0 \psi_1 \bar{\psi}_1$, as the notation suggests, and is therefore responsible for potential violation of the GN bound in Model 3.

5 Model 3 - light dark sector fermions

In this model we introduce a real scalar, ϕ, of mass m_ϕ, and two Dirac fermions, ψ_1, ψ_2, with masses m_{ψ_1, ψ_2}, where the couplings relevant for the $K \to \pi +$inv decay are

$$\mathcal{L} \supset g_{qq'}^{(\phi)}(\bar{q}_L q'_R)\phi + y_{ij}\phi\bar{\psi}_{L,i}\psi_{R,j} + \text{h.c.} \ . \tag{5.1}$$

The fermion ψ_2 is massive enough such that the decays of $K \to \pi\psi_2\bar{\psi}_2$ and $K \to \pi\psi_1\bar{\psi}_2$ are kinematically forbidden. In contrast and crucially, the decay $K \to \pi\psi_1\bar{\psi}_1$ is assumed to be kinematically allowed. The couplings of ϕ to the quarks are assumed to have a hierarchical flavor structure

$$g_{sd,ds}^{(\phi)} \ll g_{dd,ss}^{(\phi)} \ , \tag{5.2}$$

reflecting the suppression of flavor changing neutral currents of the SM, whereas the Yukawa couplings of ϕ to $\psi_{1,2}$ are assumed to favor off-diagonal transitions,

$$y_{11,22} \ll y_{12,21} \ . \tag{5.3}$$

While we do not attempt to build a full flavor model we remark in passing that such flavor structures can easily be realised within Froggatt-Nielsen (FN) type models. Choosing for instance the $U(1)_{\text{FN}}$ charges to be $[\psi_{L,2}] = [\psi_{R,2}] = 0$, $[\psi_{L,1}] = -[\psi_{R,1}] = [\phi] = 1$ and with $\epsilon = \langle\phi_{\text{FN}}\rangle/M_{\text{FN}}$ the FN spurion carrying the charge $[\epsilon] = -1$, the Yukawa and mass matrices take the form

$$y_{ij} \sim \begin{pmatrix} \epsilon^* & 1 \\ 1 & \epsilon \end{pmatrix} \ , \quad \mathcal{M}_\psi \sim m_0 \begin{pmatrix} \epsilon^2 & \epsilon \\ \epsilon & 1 \end{pmatrix} \ , \tag{5.4}$$

where the "$\sim$" sign denotes equality up to $\mathcal{O}(1)$ factors. Similarly, if $[d_{L,R}] \gg [s_{R,L}]$, the $g_{sd,ds}^{(\phi)}$ can be arbitrarily suppressed in accordance with (5.2).

Keeping the leading diagrams in y_{ij} and $g_{dd}^{(\phi)}$, shown in Fig 18, gives the following $K_L \to \pi^0 \psi_1\bar{\psi}_1$ decay amplitude

$$\mathcal{M}(K_L \to \pi^0\psi_1\bar{\psi}_1)_{\text{NP}} =$$

$$-i\bigg\{ \text{Im}\,\hat{g}_{sd}^{(\phi)} \, \text{Im}\,g_{dd}^{(\phi)} \Delta_\phi(m_K^2)\Delta_\phi(m_\pi^2)\Big[m_{\psi_2}y_{12}y_{21}\,(\bar{u}P_R v)\,\bar{\Delta} + |y_{12}|^2(\bar{u}\gamma_\mu P_L v)\bar{\Delta}^\mu\Big]B_0 f_K f_\pi$$

– 27 –

$$-\frac{\operatorname{Im}\bar{g}_{sd}^{(\phi)}}{16\pi^2}\Big[m_{\psi_2}y_{12}y_{21}\big(\bar{u}P_Rv\big)\,\mathcal{F}_L^{(\phi)}(\bar{I}_4)+|y_{12}|^2\big(\bar{u}\gamma_\mu P_Lv\big)\mathcal{F}_L^{(\phi)}(\bar{I}_4^\mu)\Big]B_0$$

$$+\operatorname{Im}\bar{g}_{sd}^{(\phi)}\,y_{11}\big(\bar{u}P_Rv\big)\Delta_\phi(q^2)\Big\}B_0+\big\{y_{ij},\gamma_5\leftrightarrow y_{ji}^*,-\gamma_5\big\}\,, \tag{5.5}$$

where $2P_{R,L}\equiv 1\pm\gamma_5$, we have shortened $\bar{u}\equiv\bar{u}(\bar{p})$, $v\equiv v(p)$, while $q^2=(p+\bar{p})^2$ is the invariant four momentum of the fermion pair. The $\bar{\Delta}^{(\mu)}$ stands for combinations of fermion propagators

$$\begin{aligned}\bar{\Delta}&=\Big[\Delta_{\psi_2}((p_\pi+\bar{p})^2)+\{\bar{p}\leftrightarrow p\}\Big]\,,\\\bar{\Delta}^\mu&=\Big[(p_\pi+\bar{p})^\mu\Delta_{\psi_2}((p_\pi+\bar{p})^2)-\{\bar{p}\leftrightarrow p\}\Big]\,,\end{aligned} \tag{5.6}$$

where $\Delta_X(k^2)$ is defined below (3.13), while $\mathcal{F}_L^{(\phi)}(Z)=\mathcal{F}_L^{(2)}(Z)\big|_{g_{qq}^{(2)}\to g_{qq}^{(\phi)}}$, with the latter defined in (3.15). Its arguments are given in terms of loop integrals,

$$\begin{aligned}\bar{I}_4(m_M)&=I_4(m_M,\bar{p})+\big\{\bar{p}\to p\big\}\,,\\\bar{I}_4^\mu(m_M)&=\big\{I_4^\mu(m_M,\bar{p})+(\bar{p}+p_\pi)^\mu I_4(m_M,\bar{p})\big\}-\big\{\bar{p}\to p\big\}\,,\end{aligned} \tag{5.7}$$

where $I_4(m_M,P)\equiv D_0(m_\pi^2,(p_\pi+P)^2,(p_K-p_\pi-P)^2,(p_K-p_\pi)^2,P^2,m_K^2,m_\phi^2,m_M^2,m_{\psi_2}^2,m_\phi^2)$ (cf. Appendix B) and I_4^μ is the same integral with an additional Lorentz-vector k^μ in the integrand.

The decay amplitude $K^+\to\pi^+\psi_1\bar{\psi}_1$ is analogous, but without the 3rd diagram in Fig. 18. This gives

$$\begin{aligned}\mathcal{M}(K^+\to\pi^+\psi_1\bar{\psi}_1)_{\mathrm{NP}}=\\-\Big\{\frac{\bar{g}_{sd}^{(\phi)}}{16\pi^2}\Big[m_{\psi_2}y_{12}y_{21}\big(\bar{u}P_Rv\big)\,\mathcal{F}_+^{(\phi)}(\bar{I}_4)+|y_{12}|^2\big(\bar{u}\gamma_\mu P_Lv\big)\mathcal{F}_+^{(\phi)}(\bar{I}_4^\mu)\Big]B_0\\-\bar{g}_{sd}^{(\phi)}y_{11}\big(\bar{u}P_Rv\big)\Delta_\phi(q^2)\Big\}B_0+\big\{y_{ij},\gamma_5\leftrightarrow y_{ji}^*,-\gamma_5\big\}\,,\end{aligned} \tag{5.8}$$

where $\mathcal{F}_+^{(\phi)}(Z)=\mathcal{F}_+^{(2)}(Z)\big|_{g_{qq}^{(2)}\to g_{qq}^{(\phi)}}$ with the later defined in (3.16). A formula for the rate, in differential form, is given in Appendix A.

5.1 Benchmarks for Model 3

The new elements of Model 3 are the Yukawa couplings between ϕ and $\psi_{1,2}$, as well as the absence of the light-scalar ϕ_1. In order to ease comparisons with Model 1 and Model 2, we use $g_{qq'}^{(2)}\to g_{qq'}^{(\phi)}$ Eqs. (3.30), (3.31)

Model 3, BM 1 : $\quad g_{dd}^{(\phi)}=\frac{(1+i)}{\sqrt{2}}g_{dd}\,,\quad \bar{g}_{sd}^{(\phi)}=\hat{g}_{sd}^{(\phi)}=\frac{(1+i)}{\sqrt{2}}g_{sd},\quad y_{12}=y_{21}=1\,, \tag{5.9}$

Model 3, BM 2 : $\quad g_{dd}^{(\phi)}=ig_{dd}\,,\quad\quad \bar{g}_{sd}^{(\phi)}=0\,,\quad \hat{g}_{sd}^{(\phi)}=ig_{sd},\quad y_{12}=y_{21}=1\,, \tag{5.10}$

while all the other couplings are set to zero. In particular, the only nonzero Yukawa couplings of ψ_i fermions for ϕ are the flavor violating ones, $y_{12,21}$, while the diagonal ones
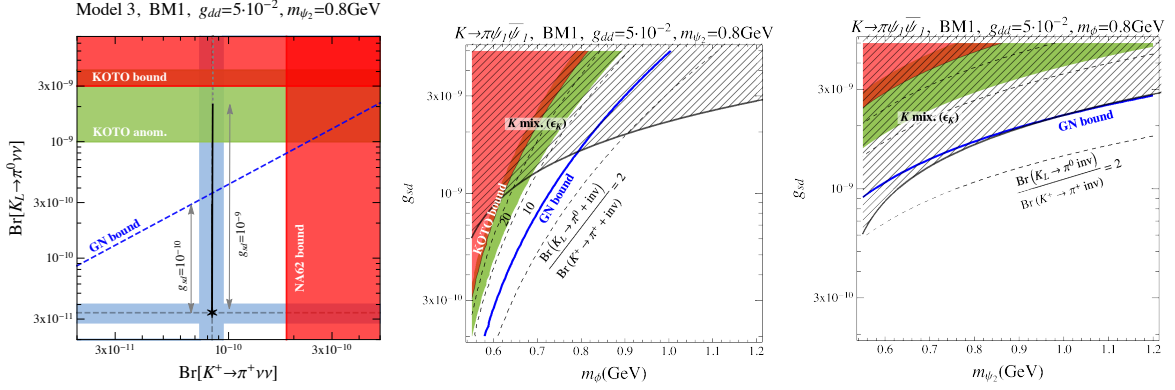
Figure 19. The parameter space for Model 3, BM1, Eq. (5.9). The color coding is the same as in Fig. 5. In the predictions for $\mathrm{Br}(K^+ \to \pi^+ + \mathrm{inv})$, $\mathrm{Br}(K_L \to \pi^0 + \mathrm{inv})$ in the left plot (black lines) we vary $m_\phi \in [0.55, 1.2]$ GeV for two values of $g_{sd} = 10^{-10}, 10^{-9}$ and fix $m_{\psi_2} = 0.8$ GeV. Right (middle) panels show the parameter space as functions of $m_{\psi_2}(m_\phi)$, fixing $m_{\phi(\psi_2)} = 0.8$ GeV.

are assumed to be vanishingly small, and set to $y_{11,22} = 0$. The mass of the lightest fermion is set to $m_{\psi_1} = 100$ MeV. The benchmarks are thus described by four continuous variables: the masses m_ϕ, m_{ψ_2} and the real parameters g_{dd}, g_{sd}.

The flavor violating coupling, $\hat{g}_{sd}^{(\phi)}$, is constrained by $K^0 - \bar{K}^0$ mixing. The bounds are the same as for ϕ_2 in Model 1, Section 3.2, and are thus obtained from Eqs. (3.29), (3.24) through the $\hat{g}_{sd}^{(2)} \to \hat{g}_{sd}^{(\phi)}$, $m_{\phi_2} \to m_\phi$ replacements. BM1 is severely constrained by ϵ_K since tree level exchange of ϕ induces a new CP violating contribution to $K^0 - \bar{K}^0$ mixing. Fig. 19 (middle) and (right) show that large enhancements of $\mathrm{Br}(K_L \to \pi^0 + \mathrm{inv})/\mathrm{Br}(K^+ \to \pi^+ + \mathrm{inv})$ are possible only for small values of m_ϕ and m_{ψ_2}, comparable to the kaon mass. Still, such light NP states are not excluded experimentally and can saturate the present KOTO bound. Fig. 19 (left) shows that in this regime it is possible to have values for this ratio well above the GN bound, in the range of the anomalous KOTO events (green band).

BM2, on the other hand, does not lead to tree level contributions to ϵ_K. The constraints from $K^0 - \bar{K}^0$ mixing are therefore relaxed compared to BM1 as they are only due to Δm_K. As shown in Fig. 20, it is thus possible to saturate the present KOTO upper bounds over a much larger set of parameter space, with masses of m_ϕ and m_{ψ_2} up to ~ 1 GeV for $g_{dd} = 5 \cdot 10^{-2}$. Next, we discuss the constraints on the ψ_1-couplings.

5.2 Constraints on the ψ_1-couplings

The leading diagrams for $\pi^0 \to \psi_1 \bar{\psi}_1$, relevant to the invisible pion constraint, are analogous to the Model 2 ones shown in Fig. 12 with $\phi_2 \to \phi$, $\phi_1 \to \psi_1$ with a ψ_2 inserted in between the final state pair in the loop diagram. Assuming $m_{\phi,\psi_2} \gg m_{\pi,\eta}$, the corresponding matrix element reads

$$\mathcal{M}(\pi^0 \to \psi_1 \bar{\psi}_1) = (\bar{u} P_R v) \frac{B_0 f}{m_\phi^2} \hat{\mathcal{M}} + \{y_{ij}, \gamma_5 \leftrightarrow y_{ji}^*, -\gamma_5\} + \mathcal{O}(m_\pi^2/m_{\phi,\psi_2}^2), \qquad (5.11)$$
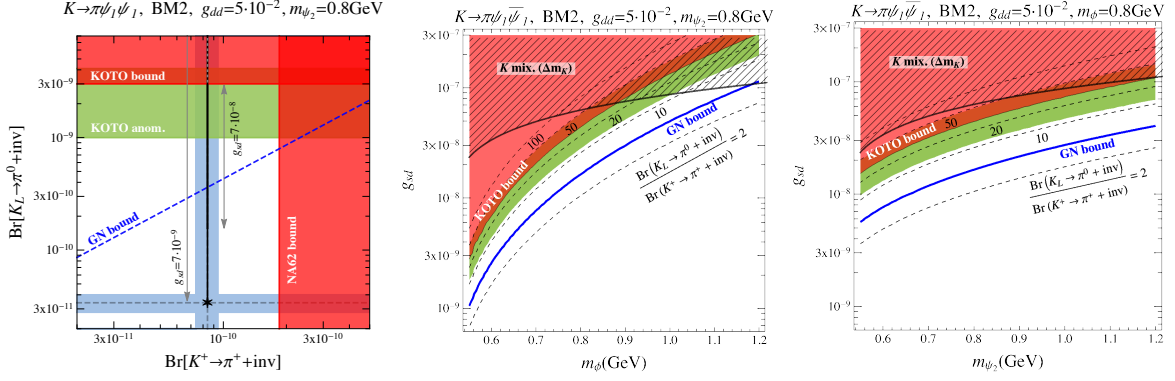
Figure 20. Same as Fig. 19 but for Model 3 BM2. In the predictions for $\mathrm{Br}(K^+ \to \pi^+ + \mathrm{inv})$, $\mathrm{Br}(K_L \to \pi^0 + \mathrm{inv})$ in the left plot (black lines) we vary $m_\phi \in [0.55, 1.2]$ GeV for two values of $g_{sd} = 7 \cdot 10^{-9}, 7 \cdot 10^{-7}$ and fix $m_{\psi_2} = 0.8$ GeV.

where $\hat{\mathcal{M}}$ is a shorthand for

$$\hat{\mathcal{M}} = \mathrm{Im}\, g_{dd}^{(\phi)} y_{11} + \mathrm{Re}\, g_{dd}^{(\phi)} y_{12} y_{21} \frac{1}{12\pi^2} \frac{B_0}{m_{\psi_2}} \left(2\,\mathrm{Im}\, g_{dd}^{(\phi)} - \mathrm{Im}\, g_{ss}^{(\phi)} \right) H(x)\,, \qquad (5.12)$$

where $x = m_\phi^2/m_{\psi_2}^2$, $H(x) = (1 + x(\ln x - 1))/(1-x)^2$ quoting $H(0) = 1$ and $H(1) = 0.5$ as representatitve values. The total rate is easily obtained from the matrix element squared given in (A.4) and the $1 \to 2$ decay rate (3.33) (without the symmetry factor $1/2$)

$$\Gamma(\pi^0 \to \psi_1 \bar{\psi}_1) = \frac{(B_0 f_\pi)^2}{m_\phi^4} \left(\beta_{\psi_1}^2 (\mathrm{Re}\, \hat{\mathcal{M}})^2 + (\mathrm{Im}\, \hat{\mathcal{M}})^2 \right) \frac{m_\pi}{16\pi} \beta_{\psi_1}\,, \qquad (5.13)$$

replacing $f \to f_\pi/\sqrt{2}$ and adapting $\beta_{\psi_1} = (1 - 4m_{\psi_1}^2/m_\pi^2)^{1/2}$. Assuming $\mathrm{Im}\, g_{ss}^{(\phi)} = 0$, $m_{\psi_1} = 0$ and $H(x) \to 1$ one gets values

$$\mathrm{Br}(\pi^0 \to \psi_1 \bar{\psi}_1) = \begin{cases} 2.6 \cdot 10^{-9} \left(\frac{|y_{11}|}{5\cdot10^{-6}} \right)^2 \left(\frac{\mathrm{Im}\, g_{dd}^{(2)}}{5\cdot10^{-2}} \right)^2 \left(\frac{\mathrm{GeV}}{m_\phi} \right)^4\,, & y_{12} y_{21} = 0\,, \\[3mm] 3.3 \cdot 10^{-9} \left(\frac{|y_{12} y_{21}|}{10^{-2}} \right)^2 \left(\frac{\mathrm{Re}\, g_{dd}^{(2)}}{5\cdot10^{-2}} \frac{\mathrm{Im}\, g_{dd}^{(2)}}{5\cdot10^{-2}} \right)^2 \left(\frac{\mathrm{GeV}}{m_\phi} \right)^4 \left(\frac{4\,\mathrm{GeV}}{m_{\psi_2}} \right)^2\,, & y_{11} = 0\,, \end{cases}$$
$$(5.14)$$

which are close to the upper experimental bound $\mathrm{Br}(\pi^0 \to \phi_1 \phi_1) < 4.4 \times 10^{-9}$ [8]. Clearly the tree graph is leading and imposes a constrain $|y_{11}| \lesssim \mathcal{O}(5 \cdot 10^{-6})$ on the Yukawa couplings to the light fermion for the two benchmarks in Figs. 19 and 20. We observe that, for both BM1 and BM2 the lightest fermion is required to be heavy enough that invisible pion decay is kinematically forbidden, $m_{\psi_1} \gtrsim m_{\pi^0}/2$. Reducing somewhat the value of $|y_{12} y_{21}| \sim \mathcal{O}(10^{-2})$, very light ψ_1 are possible. Even in this case the KOTO bounds could be saturated (at least for the BM2 flavor structure of the couplings).

5.3 ψ_1 as a dark matter candidate

In the minimal version of Model 3, presented in this work, ψ_1 and ψ_2 are odd under the Z_2-parity. The lightest fermion, ψ_1 can thus be a DM candidate. The situation is similar

to Model 2. For ψ_1 in the mass range 135 MeV $\lesssim m_{\psi_1} \lesssim$ 181 MeV, $\psi_1 \bar{\psi}_1 \to \pi^0 \pi^0$ is kinematically allowed, and can lead to the correct relic DM abundance. For lighter ψ_1 only the $\psi_1 \bar{\psi}_1 \to \gamma\gamma$ annihilation is allowed. However, if ϕ were to couple to electrons or neutrinos, the resulting annihilation cross sections can be large enough such that ψ_1 can be the DM.

For now, let us assume that $\psi_1 \bar{\psi}_1 \to \pi^0 \pi^0$ is kinematically allowed. Then at leading order there are two relevant diagrams as shown in Fig. 17. The corresponding matrix element reads

$$\mathcal{M}(\psi_1 \bar{\psi}_1 \to \pi^0 \pi^0) = \left(B_0 f \operatorname{Im} g_{dd}^{(\phi)} \Delta_\phi(m_\pi^2) \right)^2 \left[m_{\psi_2} y_{12} y_{21} \tilde{\Delta} \left(\bar{v} P_R u \right) + |y_{12}|^2 \tilde{\Delta}^\mu \left(\bar{v} \gamma_\mu P_L u \right) \right]$$
$$+ B_0 \operatorname{Re} g_{dd}^{(\phi)} \left[y_{11} \Delta_\phi(s) \bar{v} P_R u \right] + \left\{ y_{ij}, \gamma_5 \leftrightarrow y_{ji}^*, -\gamma_5 \right\} , \tag{5.15}$$

where $\bar{v} \equiv \bar{v}(p)$, $u \equiv u(\bar{p})$, $s \equiv q^2 = (p + \bar{p})^2$, and by crossing symmetry from the right diagram in Fig. 18: $\tilde{\Delta}^{(\mu)} = \bar{\Delta}^{(\mu)}|_{p,\bar{p}\to-\bar{p},-p}$ in (5.6). The cross section is obtained from the spin-averaged squared matrix element (including a symmetry factor for identical final states)

$$\frac{d\sigma}{d\Omega} = \frac{|\overline{\mathcal{M}}|^2}{512\pi^2 s} \frac{\beta_\pi}{\beta_{\psi_1}} , \tag{5.16}$$

where $\beta_{\pi,\psi_1} = (1 - 4m_{\pi,\psi_1}^2/s)^{1/2}$ are the respective velocities in the centre of mass frame. The thermally averaged cross section at leading order in the non-relativistic expansion is given by

$$\langle \sigma v \rangle = \frac{p_\pi}{32\pi m_{\psi_1}} |P|^2 , \tag{5.17}$$

where in this approximation $p_\pi = (m_{\psi_1}^2 - m_\pi^2)^{1/2}$, and

$$P = i\{ B_0 \operatorname{Re} g_{dd}^{(\phi)} \Delta_\phi(4m_{\psi_1}^2) \operatorname{Im} y_{11} +$$
$$\left(B_0 f_\pi \operatorname{Im} g_{dd} \Delta_\phi(m_\pi^2) \right)^2 \Delta_{\psi_2}(m_\pi^2 - m_{\psi_1}^2) m_{\psi_2} \operatorname{Im} y_{21} y_{12} \} , \tag{5.18}$$

is the pseudoscalar part in (A.3). It is easily obtained from (5.15) taking into account that that the role of u and v are interchanged. All other contributions, such as $|S|^2$, vanish in the non-relativistic approximation. And for values of input parameters, $y_{11} = 0$, $m_{\psi_1} = 160$ MeV, and $m_\phi = 1$ GeV one obtains a total cross section

$$\langle \sigma v \rangle = 3 \times 10^{-26} \frac{\text{cm}^3}{\text{s}} \left(\frac{\operatorname{Im} g_{dd}^{(\phi)}}{7.5 \times 10^{-2}} \right)^4 \left(\frac{\operatorname{Im} y_{21} y_{12}}{1} \right)^2 \left(\frac{1 \text{ GeV}}{m_{\psi_2}} \right)^2 , \tag{5.19}$$

which is of the right order of magnitude to produce the required relic abundance ($1 \text{ pb} \approx 3 \cdot 10^{-26} \text{cm}^3 s^{-1}$). In quoting the dependences in (5.19), we have neglected terms of $\mathcal{O}(m_{\pi,\psi_1}^2/m_{\psi_2}^2)$.

6   Conclusions

We have presented three models that can lead to large deviations in $\mathrm{Br}(K_L \to \pi^0 + \mathrm{inv})$, while leaving $\mathrm{Br}(K^+ \to \pi^0 + \mathrm{inv})$ virtually unchanged from the SM expectation. The three models are: Model 1 where the invisible decay is the two body transition $K_L \to \pi^0 \phi_1$, Model 2 with $K_L \to \pi^0 \phi_1 \phi_1$ and Model 3 with $K_L \to \pi^0 \psi_1 \bar{\psi}_1$ three body transitions, can be viewed as representatives of a larger class of models. The scalar ϕ_1 or fermion ψ_1 that escape the detector could be replaced by a dark gauge boson, or more complicated dark sector final states, without affecting our main conclusions.

Common to all these possibilities is that in addition to the invisible final state particles (in our case ϕ_1 and ψ_1), there has to be at least one additional light mediator with a $\mathcal{O}(1\ \mathrm{GeV})$-mass in order to have large violations of the Grossman-Nir bound. In Models 1 and 2 the mediator is another scalar, ϕ_2, while in Model 3 there are two mediators, the fermion ψ_2 and scalar ϕ. The scalar mediators mix with K_L and π^0, which then leads to enhanced $\mathrm{Br}(K_L \to \pi^0 + \mathrm{inv})$ rates. The required mixings are small, and thus for large parts of parameter space the most stringent constraints are due to the present KOTO upper bound on $\mathrm{Br}(K_L \to \pi^0 + \mathrm{inv})$. If the anomalous events seen by KOTO turn out to be a true signal of new physics, then these models are natural candidates for their explanation.

In Models 2 and 3 the lightest states, ϕ_1 and ψ_1, can be dark matter candidates. For the restricted mass range $m_\pi \leq m_{\phi_1, \psi_1} \leq (m_K - m_\pi)/2$ and suitable parameter ranges these particles can be the thermal relic. For lighter ϕ_1 or ψ_1 new annihilation channels are required. For example the mediators could couple to either electrons or neutrinos, in addition to the couplings to quarks.

In the numerics we followed the principle of minimality and switched on the minimal set of couplings required for large violations of the GN bound. We took great care to ensure that the radiative corrections do not modify the assumed flavor structure and potentially invalidate our conclusions. In the future, it would be interesting to revisit our simplified models in more complete flavor models which fix all the couplings to quarks. An even more ambitious possible research direction could be to explore whether the light mediators could be tied to the SM flavor puzzle itself, e.g. along the lines of Ref. [46]. We leave this and related open questions for future investigations.

A   The $K \to \pi\psi_1\bar{\psi}_1$ decay rate

For completeness we give here the explicit expression for the $K \to \pi\psi_1\bar{\psi}_1$ differential rate in Model 3. The expressions become rather involved because of the presence of the fermions in the final states. For instance, the analytic expression for the rate can only be given as a double differential rate since both variables enter the loop diagram, cf. Fig. 18, in a non-trivial way. At the end of the appendix we also comment on how this decay defies the helicity formalism used for semileptonic and flavor changing neutral currents.

The generic double differential rate in terms of Dalitz plot variables is given by [47]

$$\frac{d^2}{dq^2 dQ^2}\Gamma(K \to \pi\psi_1\bar{\psi}_1) = \frac{1}{(2\pi)^3}\frac{1}{32m_K^3}|\mathcal{M}(K \to \pi\psi_1\bar{\psi}_1)|^2 \,, \tag{A.1}$$

where $q^2 \equiv (p + \bar{p})^2$, $Q^2 \equiv (p + p_\pi)^2$ are the kinematic variables with ranges $4m_{\psi_1}^2 < q^2 < (m_K - m_\pi)^2$ and $Q_-^2 < Q^2 < Q_+^2$, with

$$Q_\mp^2 = (E_{\psi_1} + E_\pi)^2 - (p_{\psi_1} \pm p_\pi)^2 \,, \tag{A.2}$$

$E_{\psi_1} = q/2$, $E_\pi = (m_K^2 - q^2 - m_\pi^2)/2q$ and $p_i = (E_i^2 - m_i^2)^{1/2}$.

Decomposing the matrix element $\mathcal{M}$ in terms of fermion bilinears

$$\mathcal{M} = S\bar{u}v + P\bar{u}\gamma_5 v + V^\mu \bar{u}\gamma_\mu v + A^\mu \bar{u}\gamma_\mu\gamma_5 v + T^{\mu\nu}\bar{u}\sigma_{\mu\nu}v \,, \tag{A.3}$$

the generic matrix element squared, summing over fermion polarizations, reads

$$|\mathcal{M}|^2 = 2q^2\Big\{|P|^2 + \beta_{\psi_1}^2|S|^2 + \frac{2m_{\psi_1}}{q^2}((p+\bar{p})\cdot AP^* + (p-\bar{p})\cdot VS^* + \text{h.c.}) \tag{A.4}$$
$$+ A^\mu(m_{\mu\mu'} - \beta_{\psi_1}^2 g_{\mu\mu'})A^{\mu'*} + V^\mu(m_{\mu\mu'} - g_{\mu\mu'})V^{\mu'*}$$
$$+ 2T^{\mu\nu}g_{\mu\mu'}(g_{\nu\nu'} - 2m_{\nu\nu'})T^{\mu'\nu'*} + \frac{4}{q^2}\left(iT^{\mu\nu}(m_{\psi_1}(\bar{p}-p)_\mu A_\nu^* + \bar{p}_\mu p_\nu P^*) + \text{h.c.}\right)\Big\} \,,$$

where $\sigma_{\mu\nu} = i/2[\gamma_\mu, \gamma_\nu]$, $\beta_{\psi_1} = (1 - 4m_{\psi_1}^2/q^2)^{1/2}$ and $m_{\mu\nu} \equiv 2(\bar{p}_\mu p_\nu + p_\mu \bar{p}_\nu)/q^2$. For completeness we have included the tensor current in (A.3) even though it does not appear in our models.

The conversion from a form $\mathcal{M} = L\bar{u}P_L v + R\bar{u}P_R v + L^\mu \bar{u}\gamma_\mu P_L v + R^\mu \bar{u}\gamma_\mu P_R v$, used in (4.3), to the form in (A.3) proceeds via: $S[P] = 1/2(R \pm L)$ and $V[A]^\mu = 1/2(R \pm L)^\mu$. In particular for $K_L \to \pi^0\psi_1\bar{\psi}_1$

$$S[P]_L = -iB_0\left(B_0 m_{\psi_2}\text{Re}[i\,\text{Im}](y_{12}y_{21})X_L + \text{Re}[i\,\text{Im}]y_{11}\,\text{Im}\,\bar{g}_{sd}^{(\phi)}\Delta_\phi(q^2)\right) \,, \tag{A.5}$$

$$V[A]_L^\mu = -iB_0^2/2\left(|y_{21}|^2 \pm |y_{12}|^2\right)X_L^\mu \,, \tag{A.6}$$

with $X_L \equiv \text{Im}\,\hat{g}_{sd}\bar{\Delta}f_K f_\pi - \frac{\text{Im}\,\bar{g}_{sd}}{16\pi^2}\mathcal{F}_L^{(\phi)}(\bar{I}_4)$ and $X_L^\mu = X_L|_{\bar{I}_4, \bar{\Delta} \to \bar{I}_4^\mu, \bar{\Delta}^\mu}$, whereas for $K^+ \to \pi^+\psi_1\bar{\psi}_1$ (5.8) the decomposition reads

$$S[P]_+ = B_0\left(B_0 m_{\psi_2}\text{Re}[i\,\text{Im}](y_{12}y_{21})X_+ + \text{Re}[i\,\text{Im}]y_{11}\bar{g}_{sd}^{(\phi)}\Delta_\phi(q^2)\right) \,, \tag{A.7}$$

$$V[A]_+^\mu = B_0^2/2\left(|y_{21}|^2 \pm |y_{12}|^2\right)X_+^\mu \,, \tag{A.8}$$

with $X_+ \equiv -\frac{\bar{g}_{sd}}{16\pi^2}\mathcal{F}_+^{(\phi)}(\bar{I}_4)$ and $X_+^\mu = X_+|_{\bar{I}_4 \to \bar{I}_4^\mu}$.

It seems worthwhile to point out that this decay cannot be cast in the Jacob-Wick helicity formalism, since it does not corresponds to a chain of $1 \to 2$ decays. This also applies, e.g., to the generalisation of the formalism to effective theories used for $B \to K\ell^+\ell^-$ [48]. The issue is that in Model 3 the ϕ particle breaks factorization of the fermion part and the rest in the same way as the photon does between the lepton and the quarks, cf. Section 5.3. in Ref. [48]. On a technical level, this can easily be seen from the decomposition of the vector matrix element

$$V^\mu = V^{(p)}p^\mu + V^{(\bar{p})}\bar{p}^\mu + V^{(p_\pi)}p_\pi^\mu \,, \tag{A.9}$$

which necessitates all independent momenta of the decay. In the $B \to K\ell^+\ell^-$ case, induced by the standard dimension six effective Hamiltonian and no QED or electroweak corrections, the amplitude only depends on p_π, $p + \bar{p}$ but not the difference $p - \bar{p}$. However, using such a decomposition in the expressions given above does allow in practice for a fast numerical evaluation of the differential rate thereby retaining one of the main advantages of the helicity amplitude formalism.

B Integral conventions

For convenience and clarity we collect here the conventions of the Passarino-Veltman functions [49, 50, 50, 51] used in this work. The conventions are are equivalent to those of LoopTools [50] and FeynCalc [52, 53]. The loop function used are the triangle and box integrals defined by

$$C_0(p_1^2, p_2^2, (p_1+p_2)^2, m_1^2, m_2^2, m_3^2) \equiv \int_k \frac{1}{(k^2 - m_1^2)((k+p_1)^2 - m_2^2), ((k+p_1+p_2)^2 - m_2^2)} \,, \tag{B.1}$$

and

$$D_0(m_\pi^2, (p_\pi+P)^2, (p_K-p_\pi-P)^2, (p_K-p_\pi)^2, P^2, m_K^2, m_\phi^2, m_M^2, m_{\psi_2}^2, m_\phi^2) \equiv$$
$$\int_k \frac{1}{((k+p_K)^2-m_\phi^2)((k+p_\pi)^2-m_\phi^2)((k+p_\pi+P)^2-m_{\psi_2}^2)(k^2-m_M^2)} \,, \tag{B.2}$$

respectively, with $i0$-prescription suppressed and $\int_k \equiv (2\pi\mu)^{4-d}/(i\pi^2)\int d^d k$. The arguments of the D_0 function are those appearing in Model 3 in section 5. It seems worthwhile to mention that the two-point Passarino-Veltman function does not appear in this paper and the symbol B_0 is used for a quantity related to quark condensate as stated at the beginning of Section 3.1.

References

[1] Y. Grossman and Y. Nir, Phys. Lett. **B398**, 163 (1997), arXiv:hep-ph/9701313 [hep-ph] .

[2] Y. Grossman, G. Isidori, and H. Murayama, Phys. Lett. B **588**, 74 (2004), arXiv:hep-ph/0311353 .

[3] X.-G. He, X.-D. Ma, J. Tandean, and G. Valencia, (2020), arXiv:2002.05467 [hep-ph] .

[4] T. Li, X.-D. Ma, and M. A. Schmidt, Phys. Rev. **D101**, 055019 (2020), arXiv:1912.10433 [hep-ph] .

[5] A. Buras, M. Gorbahn, U. Haisch, and U. Nierste, Phys. Rev. Lett. **95**, 261805 (2005), arXiv:hep-ph/0508165 .

[6] J. Brod, M. Gorbahn, and E. Stamou, Phys. Rev. **D83**, 034030 (2011), arXiv:1009.0947 [hep-ph] .

[7] A. J. Buras, D. Buttazzo, J. Girrbach-Noe, and R. Knegjens, JHEP **11**, 033 (2015), arXiv:1503.02693 [hep-ph] .

[8] R. Volpe, "New Result on $K^+ \to \pi^+ \nu \bar{\nu}$ from the NA62 Experiment," talk presented at Pheno2020, Pittsburgh, USA, May 2020.

[9] J. K. Ahn et al. (KOTO), Phys. Rev. Lett. **122**, 021802 (2019), arXiv:1810.09655 [hep-ex] .

[10] S. Shinohara, "Search for the rare decay $K_L \to \pi^0 \nu \bar{\nu}$ at J- PARC KOTO experiment," talk presented at KAON2019, Perugia, Italy,September 2019.

[11] T. Kitahara, T. Okui, G. Perez, Y. Soreq, and K. Tobioka, Phys. Rev. Lett. **124**, 071801 (2020), arXiv:1909.11111 [hep-ph] .

[12] T. Nomura, "E14/KOTO Status," talk given at 29th J-PARC PAC meeting, J-PARC, Japan, January 2020.

[13] M. Fabbrichesi and E. Gabrielli, (2019), arXiv:1911.03755 [hep-ph] .

[14] K. Fuyuto, W.-S. Hou, and M. Kohda, Phys. Rev. Lett. **114**, 171802 (2015), arXiv:1412.4397 [hep-ph] .

[15] G. W. S. Hou, Proceedings, (KAON 2016): Birmingham, United Kingdom, 2016, J. Phys. Conf. Ser. **800**, 012024 (2017), arXiv:1611.09673 [hep-ph] .

[16] D. Egana-Ugrinovic, S. Homiller, and P. Meade, (2019), arXiv:1911.10203 [hep-ph] .

[17] P. S. B. Dev, R. N. Mohapatra, and Y. Zhang, Phys. Rev. **D101**, 075014 (2020), arXiv:1911.12334 [hep-ph] .

[18] Y. Jho, S. M. Lee, S. C. Park, Y. Park, and P.-Y. Tseng, (2020), arXiv:2001.06572 [hep-ph] .

[19] J. Liu, N. McGinnis, C. E. M. Wagner, and X.-P. Wang, (2020), arXiv:2001.06522 [hep-ph] .

[20] J. M. Cline, M. Puel, and T. Toma, (2020), arXiv:2001.11505 [hep-ph] .

[21] Y. Liao, H.-L. Wang, C.-Y. Yao, and J. Zhang, "An imprint of a new light particle at koto?" (2020), arXiv:2005.00753 [hep-ph] .

[22] G. Hiller and R. Zwicky, JHEP **03**, 042 (2014), arXiv:1312.1923 [hep-ph] .

[23] N. H. Christ, X. Feng, A. Juttner, A. Lawson, A. Portelli, and C. T. Sachrajda, Phys. Rev. **D94**, 114516 (2016), arXiv:1608.07585 [hep-lat] .

[24] J. Gasser and H. Leutwyler, Nucl. Phys. **B250**, 465 (1985).

[25] A. Pich, Rept. Prog. Phys. **58**, 563 (1995), arXiv:hep-ph/9502366 [hep-ph] .

[26] S. Aoki et al. (Flavour Lattice Averaging Group), (2019), arXiv:1902.08191 [hep-lat] .

[27] M. Tanabashi et al. (Particle Data Group), Phys. Rev. **D98**, 030001 (2018).

[28] F. Mescia and C. Smith, Phys. Rev. D **76**, 034017 (2007), arXiv:0705.2025 [hep-ph] .

[29] S. Adler et al. (E949, E787), Phys. Rev. **D77**, 052003 (2008), arXiv:0709.1000 [hep-ex] .

[30] A. J. Buras, D. Guadagnoli, and G. Isidori, Phys. Lett. **B688**, 309 (2010), arXiv:1002.3612 [hep-ph] .

[31] J. Brod, M. Gorbahn, and E. Stamou, (2019), arXiv:1911.06822 [hep-ph] .

[32] M. Bona et al. (UTfit), JHEP **03**, 049 (2008), arXiv:0707.0636 [hep-ph] .

[33] U. Collaboration, http://www.utfit.org/UTfit/, summer 2018 results.

[34] A. V. Artamonov et al. (BNL-E949), Phys. Rev. **D79**, 092004 (2009), arXiv:0903.0030 [hep-ex] .

[35] G. Ruggiero, "Latest measurement of $K^+ \to \pi^+ \nu \bar{\nu}$ with the NA62 experiment at CERN," talk presented at KAON2019, Perugia, Italy,September 2019.

[36] A. Artamonov et al. (E949), Phys. Rev. D **72**, 091102 (2005), arXiv:hep-ex/0506028 .

[37] W. Altmannshofer, S. Gori, and D. J. Robinson, (2019), arXiv:1909.00005 [hep-ph] .

[38] J. Jaeckel and M. Spannowsky, Phys. Lett. **B753**, 482 (2016), arXiv:1509.00476 [hep-ph] .

[39] E. E. Jenkins and A. V. Manohar, Phys. Lett. **B255**, 558 (1991).

[40] F. Bishara, J. Brod, B. Grinstein, and J. Zupan, JHEP **11**, 059 (2017), arXiv:1707.06998 [hep-ph] .

[41] H. Simma, Z. Phys. C **61**, 67 (1994), arXiv:hep-ph/9307274 .

[42] J. S. Lee, (2018), arXiv:1808.10136 [hep-ph] .

[43] N. Bar, K. Blum, and G. D'Amico, (2019), arXiv:1907.05020 [hep-ph] .

[44] D. Cadamuro and J. Redondo, JCAP **1202**, 032 (2012), arXiv:1110.2895 [hep-ph] .

[45] G. Bertone, D. Hooper, and J. Silk, Phys. Rept. **405**, 279 (2005), arXiv:hep-ph/0404175 [hep-ph] .

[46] A. Smolkovič, M. Tammaro, and J. Zupan, JHEP **10**, 188 (2019), arXiv:1907.10063 [hep-ph] .

[47] C. Patrignani et al. (Particle Data Group), Chin. Phys. **C40**, 100001 (2016).

[48] J. Gratrex, M. Hopfer, and R. Zwicky, Phys. Rev. **D93**, 054008 (2016), arXiv:1506.03970 [hep-ph] .

[49] G. Passarino and M. J. G. Veltman, Nucl. Phys. **B160**, 151 (1979).

[50] T. Hahn and M. Perez-Victoria, Comput. Phys. Commun. **118**, 153 (1999), arXiv:hep-ph/9807565 [hep-ph] .

[51] H. H. Patel, Comput. Phys. Commun. **197**, 276 (2015), arXiv:1503.01469 [hep-ph] .

[52] R. Mertig, M. Bohm, and A. Denner, Comput. Phys. Commun. **64**, 345 (1991).

[53] V. Shtabovenko, R. Mertig, and F. Orellana, Comput. Phys. Commun. **207**, 432 (2016), arXiv:1601.01167 [hep-ph] .